Inorganic Chemistry

Article

pubs.acs.org/IC

Ruthenium(II) and Osmium(II) Mixed Chelates Based on Pyrenyl–Pyridylimidazole and 2,2′-Bipyridine Ligands as Efficient DNA Intercalators and Anion Sensors

Sourav Mardanya, Srikanta Karmakar, Dinesh Maity, and Sujoy Baitalik*

Department of Chemistry, Inorganic Chemistry Section, Jadavpur University, Kolkata 700032, India

Supporting Information

ABSTRACT: We report herein the synthesis and characterization of two monometallic ruthenium(II) and osmium(II) complexes of composition $[(bpy)_2M(HImzPPy)](ClO_4)_2$ derived from pyrenylimidazole–10-pyridin-2-yl-9*H*-9,11-diazacyclopenta[*e*]pyrene (HImzPPy) and 2,2′-bipyridine (bpy) ligands. X-ray crystallographic study shows that both crystals belong to the triclinic system having space group $P\bar{1}$. The photophysical properties of **1** and **2** in acetonitrile indicate that the metal-to-ligand charge-transfer excited state is mainly centered in the $[M(bpy)_2]^{2+}$ moiety of the complexes and slightly affected by the extended conjugation of the pyrenylimidazole moiety. Both complexes display one-electron reversible metal-centered oxidative processes and a number of quasi-reversible reductive processes. The binding affinities of the complexes toward calf-thymus DNA (CT-DNA) were thoroughly studied through different methods such as absorption, emission, excited-state lifetime, circular dichroism, and thermal denaturation of DNA and a relative DNA binding study using ethidium bromide. All of these experiments account for the intercalative nature of both **1** and **2** toward CT-DNA as well as their light-switch behavior. The anion recognition study through different spectroscopic techniques reveals that both complexes act as "turn-on" luminescence sensors for $H_2PO_4^-$ and "turn-off" sensors toward F^- and AcO^-. The imidazole N–H proton of the receptors gets deprotonated with the excessive addition of F^- and AcO^-, while it interacts with $H_2PO_4^-$ through hydrogen-bonding interaction. Theoretical calculations (DFT and TD-DFT) were also performed to understand the photophysical properties of the metalloreceptors.

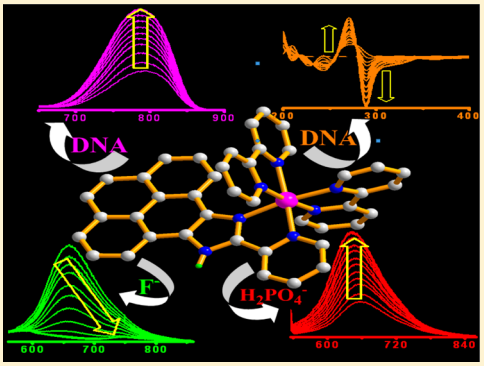

INTRODUCTION

Ruthenium(II) and osmium(II) compounds derived from polyheterocyclic ligands continue to receive increasing attention in various fields of research such as artificial photosynthesis and the development of DNA-targeted drugs and sensors because of their outstanding photoredox properties such as strong absorption and emission bands at higher wavelengths with long triplet metal-to-ligand charge-transfer (^{3}MLCT) lifetimes.[1−8] Among these complexes, those possessing desirable DNA binding abilities are particularly interesting because of their potential in the development of DNA molecular light switches, cellular imaging agents, and anticancer drugs.[4−27] Barton et al. first successfully demonstrated that an almost nonluminescent $[Ru(bpy)_2(dppz)]^{2+}$ complex in aqueous media exhibits strong luminescence in the presence of DNA and thus showed the "molecular light-switch behavior" of the complex.[9−12] Since the first report of Barton, significant efforts have been given toward designing new light-switch complexes of ruthenium(II) and osmium(II) for DNA.[13−27] One of the important characteristics of these complexes is that they possess at least one ligand having an extensive π-delocalized planar structure, which is crucial for intercalation. Among various modes of binding such as electrostatic and groove, intercalation is considered to be the most useful mode of interaction for many important applications. In our endeavor to design luminescent ruthenium(II) and osmium(II) complexes derived from a π-delocalized planar moiety, we recently designed a ditopic ligand, 10-pyridin-2-yl-9*H*-9,11-diazacyclopenta[*e*]pyrene (HImzPPy), in which a pyridylimidazole unit is rigidly connected to the pyrene moiety (Chart 1).[28] In the design of HImzPPy, the pyrene-4,5-dione core has been chosen because of its rigid, conjugated, and planar geometry and its interesting and rich photophysical

Chart 1

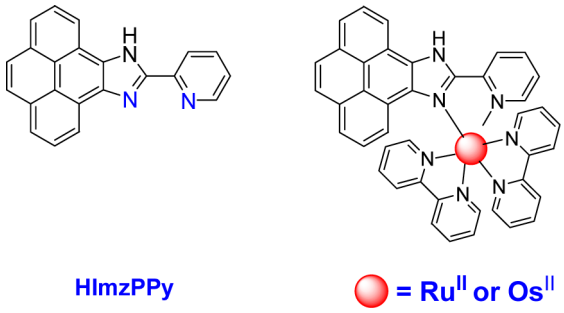

Received: September 18, 2014
Published: December 24, 2014

DOI: 10.1021/ic502271k
Inorg. Chem. 2015, 54, 513−526

properties. In this report, we have utilized this ligand for the synthesis of monometallic complexes of the type $[(bpy)_2M(HImzPPy)]^{2+}$ (M = Ru^{II} and Os^{II}). Because the imidazole moiety is an important ingredient of the purine bases in DNA, several research groups have thoroughly studied the DNA binding activities of a series of imidazole and substituted imidazole-containing polypyridine ligands and their ruthenium(II) complexes.[29−41] All of these studies addressed several important issues related to their mode of binding, site-specificity, and light-switching behaviors toward DNA.[29−41] The present work focuses on the influence of the planar pyrene moiety of the ligand on the ground- and excited-state properties as well as DNA binding abilities of the complexes. It is expected that the introduction of the pyrene moiety should increase the lifetime because it can delocalize the ^{3}MLCT lifetimes of the complexes.[42−47] Apart from excited-state delocalization, it is also expected that the introduction of the pyrene moiety can give rise to interaction between the ^{3}MLCT and triplet ($^3\pi-\pi^*$) states of pyrene, which, in turn, can also give rise to long-lived ruthenium(II) complexes, as was previously demonstrated by several research groups.[42−47] We report here the synthesis, structural characterization, photophysical properties (absorption spectra, emission spectra, and lifetime), and DNA binding and molecular light-switch behaviors of the new family of monometallic ruthenium(II) and osmium(II) complexes derived from HImzPPy. It will be seen later that, as DNA binders, our complexes have novel tilted geometry of the $M(bpy)_2$ part relative to the aromatic intercalating surface, in contrast to the C_2-symmetrical complexes in the well studied $M(L)_2$-dipyridophenazine series. Interestingly, after complexation of the ligand with the metal center, the N−H proton of the imidazole moiety becomes very acidic, a property that is very useful to recognizing selective anions in solution either through hydrogen-bonding interaction or by a proton-transfer mechanism. The topic of anion recognition contributes a lot in modern research because of its wide application in several fields such as biology, environment, and industry.[48−59] It will be demonstrated convincingly that interaction of the metal-loreceptors with DNA and selected anionic guests can give rise to substantial changes in their absorption and both steady-state and time-resolved emission spectral behaviors. Theoretical investigations [density functional theory (DFT) and time-dependent DFT (TD-DFT)] were also done to get a clear picture of the different electronic transition processes of the compounds.

EXPERIMENTAL SECTION

Materials. Calf-thymus DNA (CT-DNA), 2,2′-bipyridine (bpy), pyrene, $RuCl_3\cdot xH_2O$, $OsCl_3\cdot xH_2O$, and tetrabutylammonium (TBA) salts of the anions were procured from Sigma-Aldrich. CT-DNA was dialyzed against a 5 mM Tris buffer (pH = 7.30) until A_{260}/A_{280} was between 1.8 and 1.9, where A_{260} and A_{280} indicate the absorbance at 260 and 280 nm, respectively. Pyrene-4,5-dione,[60] *cis*-$[Ru(bpy)_2Cl_2]\cdot 2H_2O$,[61] and *cis*-$[Os(bpy)_2Cl_2]$[62] were prepared by reported procedures. 10-Pyridin-2-yl-9*H*-9,11-diazacyclopenta[*e*]pyrene (HImzPPy) ligand was synthesized and fully characterized according to a previously reported procedure by us.[28] $AgClO_4$ was prepared from silver carbonate and perchloric acid and recrystallized from benzene.

Preparation and Purification of $AgClO_4$. $AgClO_4$ was obtained by neutralizing freshly prepared silver carbonate with perchloric acid. The crude product was purified in the following way by recrystallization from benzene. A total of 1 g of crude $AgClO_4$ was dissolved in ∼6 mL of benzene and heated at reflux under a Dean−Stark apparatus until all water was removed. Then ∼5 mL of pentane was added to the solution at room temperature (RT) when a white crystalline solid appeared. The solid was separated out through filtration and kept in a vacuum desiccator containing P_2O_5. The anhydrous crystalline salt readily forms the monohydrate, which is stable at RT and therefore should be stored in a desiccator. The salt is irritating to the skin and mucous membranes, corrosive, and shock-sensitive and can be explosive in the presence of organic compounds.[63,64]

Synthesis of $[(bpy)_2Ru(HImzPPy)](ClO_4)\cdot H_2O$ (1). A mixture of *cis*-$[Ru(bpy)_2Cl_2]\cdot 2H_2O$ (0.26 g, 0.5 mmol) and $AgClO_4$ (0.20 g, 1 mmol) was refluxed in ethanol (EtOH) under a dinitrogen atmosphere for about 0.5 h. A white precipitate of AgCl that formed was removed from the resulting mixture by quick filtration. HImzPPy (0.16 g, 0.5 mmol) was then added to the filtrate containing $[Ru(bpy)_2(EtOH)_2]^{2+}$ and refluxed for 8 h. The resulting solution was filtered, and the filtrate was concentrated to ∼10 mL by rotary evaporation and kept in a refrigerator (∼5 °C) for about 12 h, when an orange-red crystalline compound precipitated. The solid product was further purified by recrystallization from a methanol MeOH−H_2O (4:1) mixture under mild acidic conditions (∼10^{-4} M $HClO_4$). Yield: 0.28 g (60%). Anal. Calcd for $C_{42}H_{31}N_7Cl_2O_9Ru$: C, 53.11; H, 3.29; N, 10.32. Found: C, 53.19; H, 3.34; N, 10.27. ^{1}H NMR (500 MHz, DMSO-d_6, TMS, δ/ppm; see Scheme 1 for atom numbering): 14.62 (s, 1H, NH), 8.93−8.79 (m, 5H, 3H3 + H9 + H13), 8.65 (d, 1H, J = 8.0 Hz, H18), 8.58 (d, 1H, J = 5.5 Hz, H3), 8.51 (d, 1H, J = 7.5 Hz, H11), 8.36−8.15 (m, 8H, 3H4 + H6 + H10 + H12 + H14 + H15), 8.04−7.99 (m, 2H, H16 + H17), 7.85 (d, 1H, J = 5.5 Hz, H6), 7.78−7.67 (m, 4H, H4 + H5 + 2H6), 7.55−7.41 (m, 3H, H5), 7.32 (t, 1H, J = 7.75 Hz, H8), 7.05 (d, 1H, J = 8 Hz, H7). ESI-MS (positive, CH_3CN): m/z 366.56 (100%; $[(bpy)_2Ru(HImzPPy)]^{2+}$), 833.11 (6%; $[(bpy)_2Ru(HImzPPy)(ClO_4)]^+$).

Scheme 1

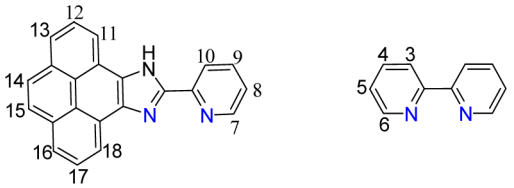

Synthesis of $[(bpy)_2Os(HImzPPy)](ClO_4)\cdot H_2O$ (2). Complex **2** was prepared by refluxing *cis*-$Os(bpy)_2Cl_2$ (0.28 g, 0.5 mmol) and HImzPPy (0.16 g, 0.5 mmol) in 100 mL of a EtOH−H_2O (1:1) mixture for ∼60 h under a dinitrogen atmosphere. After elimination of the unreacted materials, the volume of the solution was reduced to ∼20 mL by rotary evaporation and then poured into an aqueous solution (5 mL) of $NaClO_4$ (0.5 g). A dark-brown compound that formed was collected by filtration and recrystallized from a MeOH−H_2O (3:1) mixture under mild acidic conditions (∼10^{-4} M $HClO_4$). Yield: 0.29 g (57%). Anal. Calcd for $C_{42}H_{31}N_7Cl_2O_9Os$: C, 48.56; H, 3.00; N, 9.43. Found: C, 48.51; H, 3.05; N, 9.40. ^{1}H NMR (500 MHz, DMSO-d_6, TMS, δ/ppm; see Scheme 1 for atom numbering): 14.80 (s, 1H, NH), 8.85−8.79 (m, 4H, 2H3 + H9 + H13), 8.70 (d, 1H, J = 8.0 Hz, H3), 8.55−8.51 (m, 2H, H3 + H11), 8.46 (d, 1H, J = 5.5 Hz, H18), 8.30−7.99 (m, 6H, H10 + H12 + H14 + H15 + H16 + H17), 7.97−7.89 (m, 2H, H4), 7.86 (d, 1H, J = 5.5 Hz, H6), 7.74 (t, 1H, J = 8.0 Hz, H4), 7.66 (t, 1H, J = 6.5 Hz, H4), 7.62−7.58 (m, 3H, H6), 7.46 (t, 1H, J = 6.5 Hz, H5), 7.41−7.37 (m, 2H, H5), 7.35−7.28 (m, 2H, H5 + H8), 7.21 (d, 1H, J = 8.0 Hz, H7). ESI-MS (positive, CH_3CN): m/z 410.51 (100%; $[(bpy)_2Os(HImzPPy)]^{2+}$).

Caution! *Perchlorate salts of the present metal complexes are explosive so must be handled carefully in minute quantities.*

RESULTS AND DISCUSSION

Synthesis and Characterization. HImzPPy was synthesized by adopting the procedure reported by us.[28] The molecular structures of the heteroleptic ruthenium(II) and

DOI: 10.1021/ic502271k
Inorg. Chem. 2015, 54, 513−526

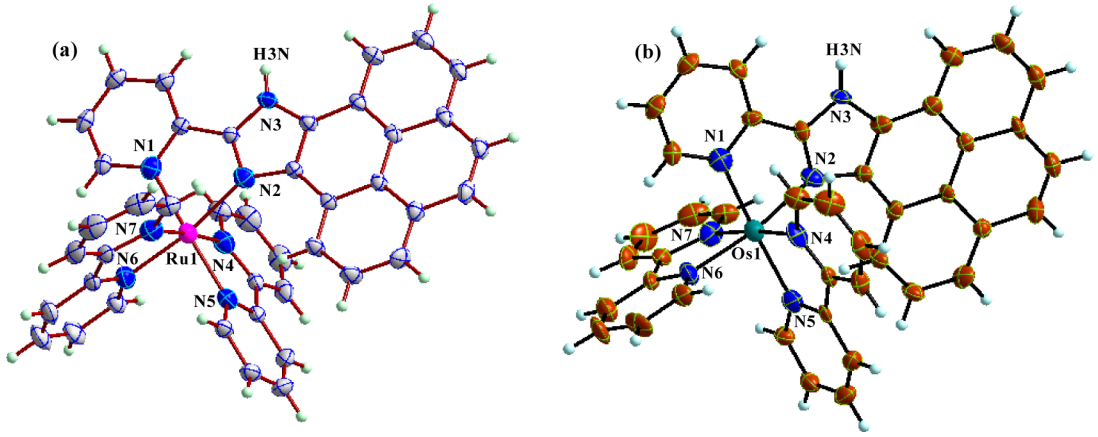

Figure 1. ORTEP representation of compounds **1** (a) and **2** (b) showing 30% probability ellipsoid plots.

Table 1. Selected Calculated Bond Distances (Å) and Angles (deg) for 1, 1a, 2, and 2a in Ground and Triplet Excited States along with the Available X-ray Crystal Data

	1						2				
	exptl	soln **1**	soln **1a**	triplet **1**	triplet **1a**		exptl	soln **2**	soln **2a**	triplet **2**	triplet **2a**
Ru1−N1	2.083(3)	2.116	2.117	2.113	2.119	Os−N1	2.075(6)	2.117	2.124	2.120	2.112
Ru1−N2	2.134(3)	2.211	2.176	2.211	2.095	Os−N2	2.120(5)	2.201	2.176	2.203	2.147
Ru1−N4	2.064(3)	2.103	2.101	2.104	2.107	Os−N4	2.063(5)	2.107	2.101	2.107	2.105
Ru1−N5	2.070(3)	2.106	2.100	2.107	2.054	Os−N5	2.069(5)	2.109	2.100	2.131	2.118
Ru1−N6	2.061(3)	2.089	2.085	2.089	2.122	Os−N6	2.067(6)	2.096	2.091	2.06	2.088
Ru1−N7	2.043(3)	2.076	2.087	2.076	2.118	Os−N7	2.058(5)	2.082	2.090	2.071	2.086
N1−Ru1−N2	78.13(11)	77.7	78.2	77.6	80.02	N1−Os1−N2	77.3(2)	77.0	77.3	77.2	78.3
N1−Ru1−N4	170.89(11)	173.7	173.0	173.7	174.3	N1−Os1−N4	170.3(2)	173.3	172.8	173.3	174.0
N1−Ru1−N5	92.56(11)	96.2	95.6	96.2	95.8	N1−Os1−N5	92.9(2)	96.5	95.9	98.0	98.4
N1−Ru1−N6	91.21(11)	88.6	88.8	88.5	87.2	N1−Os1−N6	91.2(2)	88.4	88.4	86.8	85.7
N1−Ru1−N7	94.09(11)	93.9	93.8	94.1	94.2	N1−Os1−N7	94.7(2)	94.5	94.2	93.9	93.7
N2−Ru1−N4	102.38(10)	103.3	103.2	103.2	102.8	N2−Os1−N4	103.2(2)	104.0	103.9	106.1	104.9
N2−Ru1−N5	86.85(10)	86.3	87.0	86.2	90.7	N2−Os1−N5	86.1(2)	85.7	86.4	84.6	85.8
N2−Ru1−N6	96.36(11)	97.5	96.2	97.6	97.0	N2−Os1−N6	97.6(2)	98.1	96.5	97.8	97.0
N2−Ru1−N7	171.05(11)	170.9	170.4	171.1	172.0	N2−Os1−N7	170.9(2)	170.8	170.0	170.9	171.3
N4−Ru1−N5	78.42(12)	77.7	77.7	77.6	79.3	N4−Os1−N5	77.5(2)	77.0	77.1	76.7	76.9
N4−Ru1−N6	97.75(11)	97.3	97.6	97.4	97.1	N4−Os1−N6	98.3(2)	97.8	98.4	98.1	98.6
N4−Ru1−N7	86.01(11)	85.2	85.3	85.2	83.3	N4−Os1−N7	85.4(2)	84.7	85.0	82.8	83.2
N5−Ru1−N6	175.49(10)	174.2	172.1	174.4	172.0	N5−Os1−N6	175.02(19)	173.4	174.1	174.8	175.2
N5−Ru1−N7	98.03(11)	98.2	99.0	98.2	95.4	N5−Os1−N7	98.8(2)	99.0	99.9	98.8	98.8
N6−Ru1−N7	79.22(12)	78.4	78.2	78.4	77.0	N6−Os1−N7	78.1(2)	77.7	77.5	79.2	78.6

osmium(II) complexes derived from HImzPPy are presented in Chart 1. The reaction between HImzPPy and $[(bpy)_2Ru(EtOH)_2]^{2+}$ produces the mononuclear complex of composition $[(bpy)_2Ru(HImzPPy)](ClO_4)_2$ (**1**). The analogous osmium(II) complex $[(bpy)_2Os(HImzPPy)](ClO_4)_2$ (**2**) was prepared by refluxing *cis*-$[Os(bpy)_2Cl_2]$ and HImzPPy in a mixture of EtOH−H_2O (1:1) for about 60 h. The complexes were thoroughly characterized by several techniques such as elemental (C, H, and N) analyses, high-resolution mass spectrometry, and NMR spectroscopy.

Description of the Crystal Structures of 1 and 2. Figure 1 presents the ORTEP[65] diagrams of both complexes, and the geometrical parameters are presented in Table 1. Both complexes belong to the triclinic crystal system having space group $P\bar{1}$. In the six-coordinated octahedral geometry of **1** and **2**, HImzPPy coordinates through its N2 (imidazole) and N1 (pyridyl) atoms to the $M(bpy)_2$ (M = Ru^{II} and Os^{II}) units. Moreover, the distorted octahedral geometry of the complexes was reflected in their geometrical parameters presented in Table 1. The average M−N(bpy) distances in both complexes are almost similar and lie in the range between 2.043 and 2.070 Å, whereas the M−N(imidazole) lengths [2.075(6) and 2.134(3) Å] are comparatively long. It is to be noted that the dihedral angle between the pyridyl group and pyrenylimidazole moiety is close to zero, indicating almost planar structure of the ligand in both complexes.

X-ray crystal structure analysis indicates the presence of several interactions like $\pi-\pi$, CH−π, etc., in complexes **1** and **2** (Figure S1 in the SI), and the related data are given in Table S2 in the SI. The pyridine ring of HImzPPy is in a face-to-face orientation with the phenyl group (C16−C21 atoms) of the pyrene moiety in both complexes. The two centroids are separated by a distance of 3.554 Å in **1** and 3.564 Å in **2**, which indicates the presence of $\pi-\pi$ interactions. The H40 atom in

DOI: 10.1021/ic502271k
Inorg. Chem. 2015, 54, 513−526

the pyridine ring of a bpy ligand interacts strongly with the π cloud of the adjacent pyridine ring (N4C23C24C25C26C27), and the distance of H40 from the centroid of the corresponding pyridine ring is 2.668 Å for **1** and 2.691 Å for **2**. Moreover, the perchlorate anion is located between the two complex units and forms short contacts to selective protons of the bpy moieties and imidazole N−H proton (Table S3 and Figure S2 in the SI)

Characterization of the Complexes by Electrospray Ionization Mass Spectrometry (ESI-MS) and NMR Spectra. ESI-MS and both ^{1}H and {^{1}H−^{1}H} COSY NMR spectra in $(CD_3)_2SO$ at RT confirm the structures of the complexes in the solution state. Complex **1** shows two peaks at m/z 366.56 and 833.11, and complex **2** exhibits one peak at m/z 410.51 in their ESI-MS spectra in CH_3CN (Figures S3 and S4 in the SI). The isotopic patterns and separation of 0.5 Da among the successive lines for the peak at m/z 366.56 for **1** and at m/z 410.51 for **2** correspond to the species $[(bpy)_2Ru(HImzPPy)]^{2+}$ and $[(bpy)_2Os(HImzPPy)]^{2+}$, respectively. Moreover, the peak at m/z 833.11 for **1** corresponds to $[(bpy)_2Ru(HImzPPy)(ClO_4)]^+$.

Figure S5 in the SI shows the tentative assignment of different protons in the metal complexes and the free ligand. Both complexes exhibit many resonances with some sort of overlap in the range of 7.04−8.93 ppm. The COSY spectra (Figures S6 and S7 in the SI) are very helpful to assign the protons of HImzPPy and the bpy moiety coordinated to the metals. The most downfield-shifted proton appears at 14.62 ppm for **1**, and that 14.80 ppm for **2** corresponds to the NH proton of the imidazole moiety in the complexes.

Absorption Spectra. Figure 2a shows the absorption spectra, and Table 2 presents the relevant spectral data of **1** and

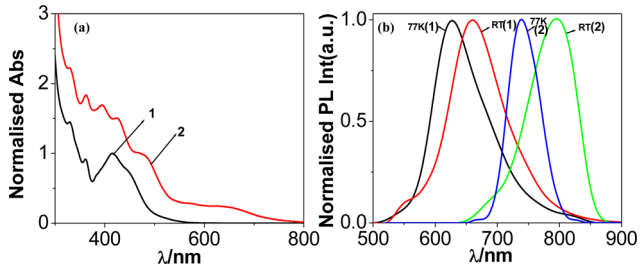

Figure 2. Normalized absorption (a) and luminescence (b) spectra of **1** and **2**.

2 in CH_3CN. The spectra of the complexes seem to be an approximate combination of each of the spectra of the $[M(bpy)_3]^{2+}$, pyrene, and imidazole moieties. The bands in the UV region originated from the $\pi-\pi^*$ transitions within the bpy and pyrenylimidazole groups, whereas the peaks in the visible range between 416 and 495 nm (ε = 20310−9577 M^{-1} cm^{-1}) are due to $^1[M^{II}(d\pi)^6] \rightarrow {}^1[M^{II}(d\pi)^5bpy(\pi^*)^1]$ and $^1[M^{II}(d\pi)^6] \rightarrow {}^1[M^{II}(d\pi)^5HImzPPy(\pi^*)^1]$ transitions.[2,3,59] For complexes of this type, one could expect two well-defined MLCT bands, but in practice we observed a single broad peak due to their small wavelength separation. Additionally, the broad band in the wavelength region of 600−700 nm for complex **2** can be assigned as spin-forbidden $^1[Os^{II}(d\pi)^6] \rightarrow {}^3[Os^{II}(d\pi)^5bpy/HImzPPy(\pi^*)^1]$ transitions.[2,3,59]

Luminescence Spectra. Figure 2b represents the emission spectra of the complexes in a fluid solution at RT and in EtOH−MeOH (4:1) glass at 77 K, and Table 2 summarizes the useful luminescence data. Upon excitation at their MLCT band, complex **1** exhibits broad bands at 658 nm (RT) and at 628 nm (77 K), while **2** shows bands at 796 nm (RT) and at 738 nm (77 K) originating from their respective ^{3}MLCT excited states.[2,3,59] Complex **1** exhibits biexponential radiative decay, with a first component lifetime of 6.8 ns followed by a long-lived second component with a lifetime of 78.0 ns. By contrast, the analogous osmium(II) complex (**2**) exhibits monoexponential decay with a lifetime of 14.5 ns. The initial short component can be assigned as due to the ^{3}MLCT state, whereas the long component arises from the excited-state equilibrium with the triplet state of the pyrene moiety, which repopulates the ^{3}MLCT state after the initial emission.[42−45] In the case of osmium, the excited-state equilibrium is not occurring probably because of the larger energy difference between the triplet states caused by stronger crystal-field strength by osmium(II) than ruthenium(II).[2,3,45,59] Similar to related ^{3}MLCT emitters, substantial enhancement of the luminescence intensity and quantum yields occurs by freezing the complexes at 77 K (Table 2).[1,6,15] The intersecting point of the absorption and luminescence spectra of the complexes can give an estimate of their excited-state energies (E_{00}). The calculated E_{00} values, 2.32 eV for **1** and 1.82 eV for **2**, are comparable to those of similar polypyridine complexes of ruthenium(II) and osmium(II).[2,3,45,59]

Temperature-Dependent Emission. To get a clear idea about the deactivation dynamics of the excited states, both steady-state and time-resolved emission spectra of the complexes have been measured by varying the temperature. The experimental findings (Figure 3) show that the emission intensity, quantum yield, and lifetime increased progressively with decreasing temperature for the ruthenium(II) complex (**1**), while for the analogous osmium(II) complex (**2**) remains almost invariant. Upon increasing temperature, radiationless decay becomes favorable for the polypyridineruthenium(II) complexes because of surface crossing between the radiative ^{3}MLCT and nonradiative ^{3}MC states, resulting in a decrease of the overall lifetime.[2,3,45] By contrast, in the osmium(II) analogues, because of the larger energy gap between the emitting ^{3}MLCT and ^{3}MC states, the emission intensity as well as the lifetime is only slightly perturbed by lowering of the temperature.[2,3,45]

Table 2. Spectroscopic and Photophysical Data for Complexes 1 and 2 in Acetonitrile

		luminescence				
		at 298 K			at 77 K	
compound	absorption λ_{max}/nm (ε/M^{-1} cm^{-1})	λ_{max}/nm	τ/ns	Φ/10^{-3}	λ_{max}/nm	Φ/10^{-2}
1	448 br (14995), 416 br (20310), 362 sh (18290), 332 sh (28935), 286 (88038), 239 (80225)	658	τ_1 = 6.8, τ_2= 78.0	1.42	628	5.16
2	654 br (2050), 495 br (9577), 362 br (14560), 290 (53400), 240 (71080)	796	τ_1 = 14.5	1.36	738	6.52

DOI: 10.1021/ic502271k
Inorg. Chem. 2015, 54, 513−526

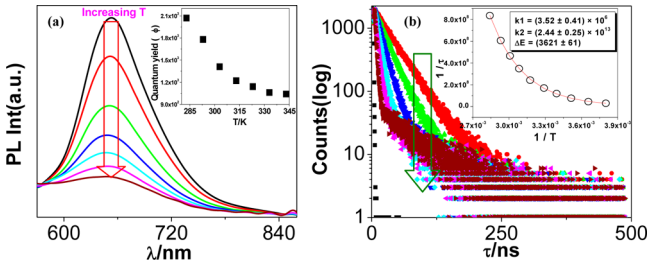

Figure 3. Effect of the temperature on steady-state emission (a) and excited-state decay profiles (b) for **1** in acetonitrile. The changes of the quantum yields with the temperature are shown in the inset of part a, while the temperature-dependent lifetime data with the values of different parameters and the corresponding nonlinear fit are shown in the inset of part b.

Equation 1 can be utilized to fit the experimental temperature versus lifetime data.[2,66]

$$\tau(T)^{-1} = [k_1 + k_2 \exp(-\Delta E_2/RT)] / [1 + \exp(-\Delta E_2/RT)] \quad (1)$$

where k_1 is the temperature-independent rate constant, which consists of both radiative (k_r) and nonradiative (k_{nr}) decay constants at low temperature (77 K). It is assumed that both k_r and k_{nr} are independent of the temperature at $T > 77$ K. The temperature-dependent rate constant k_2 represents the decay constant for accessing the ligand-field (^{3}MC) state from the ^{3}MLCT state, and the activation energy required for this process is represented as ΔE_2. The denominator in the above equation is necessary for small values of ΔE_2.[2,66] It may be noted that eq 1 forces all of the temperature dependence into a single term. The calculated values of $\Delta E_2 = 3621 \pm 61$, $k_1 = (3.52 \pm 0.41) \times 10^6$ s^{-1}, and $k_2 = (2.44 \pm 0.25) \times 10^{13}$ s^{-1} for **1** are found to correlate reasonably well with the estimated data for the related complexes.[2]

Electrochemical Properties. The electrochemical responses of **1** and **2** are represented in Figure 4, with the relevant data in Table 3. For both **1** and **2**, we get one reversible oxidative peak and three reductive peaks. Among the three reductive peaks, two are quasi-reversible and one is irreversible in nature. On the basis of the literature data, the oxidation at 1.44 V for **1** and at 1.02 V for **2** can be attributed to M^{II}/M^{III} (M = Ru and Os) processes.[2,59] Again, the Os^{II}/Os^{III}

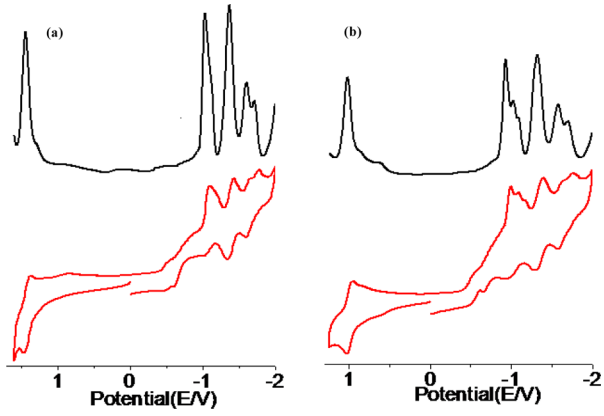

Figure 4. Full range cyclic voltammograms and square-wave voltammograms of **1** and **2** in acetonitrile at a scan rate of 100 mV/s showing both oxidation and reduction of the complexes.

Table 3. Electrochemical Data[a] for Complexes 1 and 2 in Acetonitrile

compound	oxidation $E_{1/2}$(ox)/V	reduction[b] $E_{1/2}$(red)/V
1	1.44	−1.02, −1.37, −1.75
2	1.02	−0.93, −1.32, −1.72

[a]All of the potentials are referenced against a Ag/AgCl electrode with $E_{1/2} = 0.36$ V for the Fc/Fc$^+$ couple. [b]$E_{1/2}$ values were obtained from square-wave voltammetry using a glassy carbon electrode.

couple oxidizes at less potential than the Ru^{II}/Ru^{III} couple as expected. The origin of the first reduction process in both complexes around −1.0 V is not clear to us, while the successive reduction processes observed between −1.4 and −1.8 V can be attributed to coordinated bpy and HImzPPy ligands by comparing the reduction of free HImzPPy at −1.74 V in CH_3CN.[28]

DNA Binding Studies. *UV−Vis Absorption Spectroscopy.* The changes in the UV−vis absorption spectra for the interaction of CT-DNA with the metal complexes are represented in Figure 5. The MLCT band at 416 nm and the

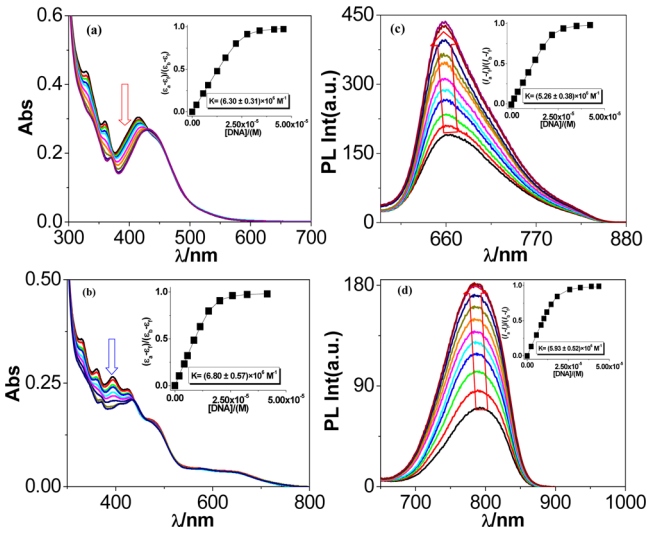

Figure 5. Changes in the UV−vis absorption (a and b) and luminescence (c and d) spectra of **1** and **2** (20 μM) in the presence of increasing amount of CT-DNA (0−43 μM for **1** and 0−40 μM for **2**) in a Tris−NaCl buffer medium (pH = 7.30). The insets show the binding profiles with DNA.

$\pi-\pi^*$ band at 360 nm get red-shifted to 433 and 370 nm, respectively, with a concomitant decrease of the intensities upon the gradual addition of CT-DNA to a solution of **1**. Moreover, in the titration process, all of the spectra go through an isosbestic point at 430 nm. Similarly, with the addition of CT-DNA to a solution of **2**, diminution of the intensities and bathochromic shifts of all of the absorption peaks were observed with concurrent development of an isosbestic point at 441 nm. It is to be noted that the incorporation of CT-DNA resulted in hypochromism in both cases. The extent of hypochromism H % (=100($A_{free} - A_{bound}$)/A_{free}) varied from 21to 37.8% for the $\pi-\pi^*$ bands and from 20.4 to 28.6% for the MLCT peaks in the complexes. With the help of eq 2 and by utilization of the titration data, the binding affinity of the metal complexes toward DNA was estimated (inset to Figure 5a,b).[67,68] The terms ε_a, ε_f, and ε_b in eq 2 corresponds to the extinction coefficient of the apparent, free, and fully bound

DOI: 10.1021/ic502271k
Inorg. Chem. 2015, 54, 513−526

forms of the complexes, while s corresponds to the size of the binding site.

$$(\varepsilon_a - \varepsilon_b)/(\varepsilon_b - \varepsilon_f) = [b - (b^2 - 2K_b{}^2C_t[\mathrm{DNA}]/s)^{1/2}]/2K_bC_t \quad (2)$$

$$b = 1 + K_bC_t + K_b[\mathrm{DNA}]/2s$$

By monitoring the spectral changes at 382 nm for **1** and 394 nm for **2**, we calculated $K_b = (6.30 \pm 0.31) \times 10^6\ M^{-1}$ and $s = 1.51 \pm 0.06$ for **1** and $K_b = (6.80 \pm 0.57) \times 10^6\ M^{-1}$ and $s = 1.54 \pm 0.01$ for **2** (insets of Figure 5). Thus, the large hypochromism and the shifts of the absorption peaks toward higher wavelength along with high values of the binding constants indicate intercalation of the complexes into the DNA base pairs.[69] It is to be noted that the large hypochromism of the absorption bands and high K_b values of our complexes resemble well with that of the classical DNA intercalators, e.g., Δ-$[Ru(phen)_2(dppz)]^{2+}$ and Λ-$[Ru(phen)_2(dppz)]^{2+}$, which exhibit hypochromism of 32.1% (372 nm) and 29.8% (372 nm) and K_b values of 1.7×10^6 and $3.2 \times 10^6\ M^{-1}$, respectively.[70] Moreover, the strong binding and intercalative behaviors of the metalloreceptors with CT-DNA may be attributed to the synergistic contributions of a rigid, planar, and extensively π-delocalized pyrene system and increased hydrophobicity imparted by the introduction of an imidazole ring to the complex systems because the bpy moiety was previously shown to be inefficient for intercalative binding with DNA.[69]

Emission Spectroscopy. The binding of **1** and **2** toward CT-DNA has also been studied by emission spectroscopy. In the absence of CT-DNA, both complexes emitted relatively weakly in an aqueous buffer solution. The additive effect of CT-DNA to the Tris buffer solution of the complexes is presented in Figure 5c,d. Upon the addition of CT-DNA, the emission intensity of the peak at 663 nm for **1** increased sharply with an enhancement factor of 2.3, with the corresponding emission quantum yield being 140% (λ_{em} = 663 nm). For the osmium(II) complex (**2**), the augmentation of the emission intensity at 794 nm is slightly greater (factor of 2.5), with the emission quantum yield being 145% (λ_{em} = 794 nm). It is of interest to note that the DNA-induced luminescence enhancement factors for the complexes are comparable to those of $[Ru(phen)_2phehat]^{2+}$,[70] $[Ru(phen)_2(dicnq)]^{2+}$,[25] $[Ru(bpy)_2tpphz]^{2+}$,[72] $[Ru(phen)_2\ dppx]^{2+}$,[73] and $[Ru(phen)_2dpqa]^{2+}$[73] but much less than the factor of $\sim 10^4$ observed for $[Ru(bpy)_2dppz]^{2+}$ and $[Ru(phen)_2dppz]^{2+}$.[9] Thus, the present complexes can be regarded as a new class of light switches for DNA as the emission intensities of the complexes get significantly enhanced in the presence of DNA. The substantial enhancement of the emission intensity of the receptors in the presence of CT-DNA could be due to their intercalation property. Moreover, this intercalation to the DNA base pairs imparts rigidity in the system, causing the diminution of nonradiative decays.[9−15,24−26,74] The changes in the emission profiles were utilized to determine the binding affinities of the complexes toward CT-DNA by using eq 3.[75]

$$(I_a - I_f)/(I_b - I_f) = [b - (b^2 - 2K_b{}^2C_t[\mathrm{DNA}]/s)^{1/2}]/2K_bC_t \quad (3)$$

where $b = 1 + K_bC_t + K_b[\mathrm{DNA}]/2s$.

A plot of $(I_a - I_f)/(I_b - I_f)$ versus [CT-DNA] gives rise to the values of $K_b = (5.26 \pm 0.38) \times 10^6\ M^{-1}$ and $s = 1.15 \pm 0.07$ for **1** and $K_b = (5.93 \pm 0.52) \times 10^6\ M^{-1}$ and $s = 1.45 \pm 0.01$ for **2**. The values of K_b obtained from absorption and emission titration data agree reasonably well with each other and are also comparable with that of well-established DNA intercalators such as $[Ru(phen)_2(dppz)]^{2+}$ [$2.1 \times 10^6\ M^{-1}$ (s = 2.4)].

In order to check the site specificity, we have carried out luminescence titrations of the metalloreceptors (**1** and **2**) with $[poly(dA\text{-}dT)_2]$ and $[poly(dG\text{-}dC)_2]$, and we have also calculated their binding constants toward these polynucleotides by fitting the emission titration data (Figures S8 and S9 and Table S4 in the SI). Although the binding constants of the complexes toward $[poly(dG\text{-}dC)_2]$ are little bit higher compared to those of $[poly(dA\text{-}dT)_2]$, the extent of the difference is rather small. Thus, the values of the binding constants suggest no preferential binding of the complexes for the GC or AT site.

Emission Lifetimes. The excited-state lifetimes of receptors **1** and **2** were measured with varying amounts of CT-DNA for a better understanding of their intercalative nature (Figure 6). It

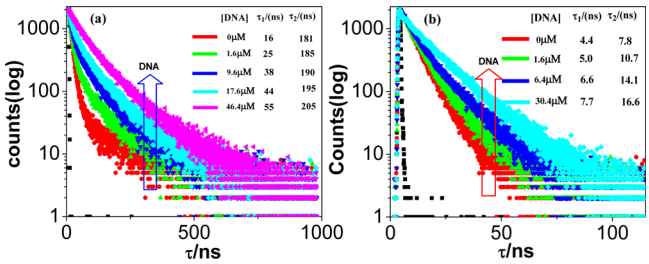

Figure 6. Changes in the time-resolved luminescence decay of **1** (a) and **2** (b) with increasing amount of CT-DNA (0−46 μM for **1** and 0−30 μM for **2**) in a Tris−NaCl buffer medium (pH = 7.30).

is observed that both complexes exhibit biexponential decay in the absence of CT-DNA. Upon increasing concentration of CT-DNA, the lifetimes of both components increase significantly (τ_1, 16 → 55 ns for **1** and 4.4 → 7.7 ns for **2**; τ_2, 181 → 205 ns for **1** and 7.8 → 16.6 ns for **2**) with an overall increase in the lifetime in both cases.[9−15,24−26,74] As already mentioned, intercalation with CT-DNA can lead to rigidity in the system, which, in turn, increases the luminescence lifetimes of the complexes. Moreover, the change of the surrounding solvent structures may also be the reason for enhancement of the lifetimes. So, the long-lifetime components probably arise from intercalation of the complexes to DNA, while the short-lifetime components may correspond to free metal complexes as well as their surface-bound forms.

Ethidium Bromide (EB) Displacement Studies. EB is a well-established DNA intercalator. If our complexes displace EB from CT-DNA−EB conjugate, we can obtain indirect evidence of the intercalative binding mode of the complexes with DNA. We have monitored this displacement reaction by means of fluorescence spectroscopy. The addition of either **1** or **2** to the solution of CT-DNA pretreated with EB should displace EB. As a result, the emission intensity of EB will be drastically reduced because free EB does not show any fluorescence in an aqueous medium.

Moreover, free **1** and **2** and DNA-bound **1** and **2** also fluoresce very weakly at the excitation wavelength λ_{ex} = 546 nm. Figure 7 represents the changes in luminescence spectral behaviors for EB emission (λ_{ex} = 546 nm) with increasing concentration of the complexes to the DNA-bound EB system. In both cases, dramatic reductions of EB emission intensities

DOI: 10.1021/ic502271k
Inorg. Chem. 2015, 54, 513−526

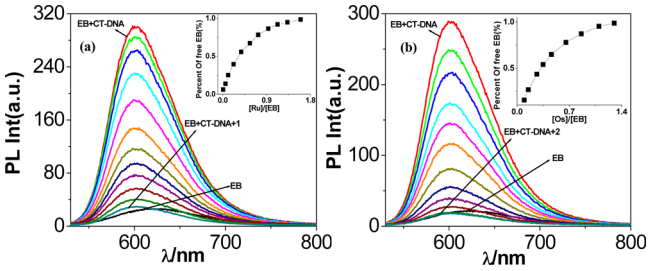

Figure 7. Emission spectra of EB bound to DNA in the presence of the incremental addition of **1** (a) and **2** (b) in a Tris−NaCl buffer medium (pH = 7.30). The insets show plots of the percentage of free EB versus [Ru/Os]/[EB].

(97.8% for **1** and 99.5% for **2**) occur. The results of the displacement experiments reveal that the present complexes are strong DNA intercalators because they almost completely displace the EB molecules from CT-DNA−EB conjugate and not partially, which is usually with DNA groove binders.[77] Moreover, the emission titration data lead us to calculate the apparent binding constants of the complexes toward CT-DNA with the help of eq 4.[41,78]

$$K_{app} = K_{EB}[EB]_{50\%}/[Ru/Os]_{50\%} \quad (4)$$

The terms K_{app} and K_{EB} represents the apparent DNA binding constant of **1** and **2** and the binding constant of EB bound to DNA, while $[EB]_{50\%}$ and $[Ru/Os]_{50\%}$ are the concentrations of EB and the complexes when the fluorescence is reduced to 50%. From the plots, it is evident that half of the EB molecules stuck to DNA have been replaced at a concentration ratio of [Ru]/[EB] = 0.33 for **1** and [Os]/[EB] = 0.31 (inset to Figure 7). It may be mentioned that the DNA binding constants of EB reported in this way vary considerably,[79] and the displacement of EB by the incoming molecule may not always follow 1:1 stoichiometry, both of which could complicate the use of a competitive binding model for establishing DNA binding constants. By taking a K_{EB} value of 1.25×10^6,[41] the calculated apparent binding constants (K_{app}) are 3.78×10^6 for **1** and 4.03×10^6 M^{-1} for **2**.

Circular Dichroism (CD). The strong interaction between the complexes and CT-DNA was also evidenced from CD measurements. The present complexes do not show any CD band because they are achiral in nature. The B form of CT-DNA exhibits two bands at 273 and 242 nm in its CD spectrum due to base stacking and helicity, respectively. Moreover, the intercalators show induced CD peaks when they bind with the DNA helix.[80] Figure 8 depict the changes in the CD spectral profiles of CT-DNA with both **1** and **2**. With increasing

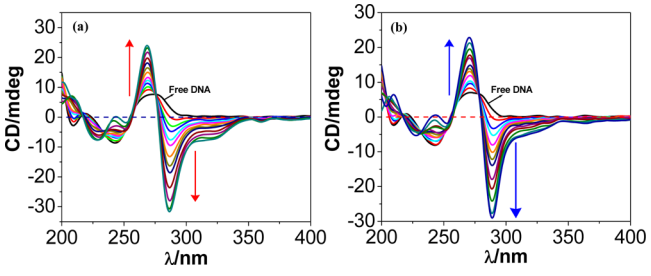

Figure 8. Changes in the CD spectra of CT-DNA (60 μM) with increasing concentration of **1** (0−35 μM) (a) and **2** (0−30 μM) (b) in a Tris−NaCl buffer medium (pH = 7.30).

concentration of **1**, it is observed that the intensity of the positive band at 268 nm continued to increase while the positive band at 285 diminished gradually with concomitant development of a negative band at the same position until the complex concentration reaches around 35 μM. The band at 242 nm also increases in intensity in this interaction process, albeit to a small extent. The osmium(II) compound (**2**) also displays similar spectral changes with diminution of the peak at 288 nm and simultaneous enhancement of the peak at 270 nm. The induced CD peaks arise because of changes in absorption as the metal complexes intercalated into the DNA base pairs.[81,82]

DNA Melting Curves. Generally, the DNA melting temperature (T_m) increases in the presence of both intercalators and a minor groove binder because their binding to DNA stabilizes its double-helical structure.[77] T_m can be measured by performing the variable-temperature absorbance study of CT-DNA. From the sigmoidal melting curve as presented in Figure 9, we can

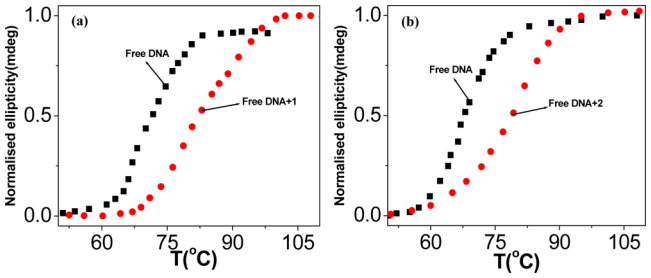

Figure 9. Thermal melting curve of CT-DNA in free and bound conditions to **1** (a) and **2** (b) in a Tris−NaCl buffer medium (pH = 7.30).

calculate T_m for **1** and **2** when half of the DNA molecules get separated from their double-stranded orientation. It is evident that free DNA melts at 67 °C, whereas the addition of the metal complexes leads to an increase in the T_m value by 12 °C for **1** and by 15 °C for **2** owing to stabilization of the double-helical structure of DNA. By comparison of the previous literature data, it is suggested that an intercalative binding of both **1** and **2** to DNA occur. It is of interest to note that the osmium(II) compound (**2**) shows more affinity to bind with DNA than the ruthenium(II) compound (**1**), as evidenced from its higher T_m value and also from its higher binding constant values calculated from UV−vis absorption and emission spectroscopy measurements. This is not unexpected because the increase in size of the metal induces a larger crystal field and causes the resulting complex to be more planar than its ruthenium(II) analogue, inducing greater capability of the pyrenylimidazole moiety to intercalate into the DNA base pairs.

Selective Anion-Sensing Features of 1 and 2. The potential application of complexes containing one imidazole NH group in their framework of a coordinated pyridylpyrene ligand toward the recognition and sensing of selective anion(s) has been evaluated through different experimental techniques and DFT calculations. The initial assessment of the anion recognition property was qualitatively investigated by observing the visible color changes of the receptors in an acetonitrile solution in the presence of TBA salts of F^-, Cl^-, Br^-, I^-, NO_3^-, HSO_4^-, AcO^-, $H_2PO_4^-$, and OH^- ions. The photographs in the insets of Figure 10a,b show distinct color changes of **1** and **2** mainly with F^- and OH^-, while with the other anions, the visible color remains almost unchanged.

DOI: 10.1021/ic502271k
Inorg. Chem. 2015, 54, 513−526

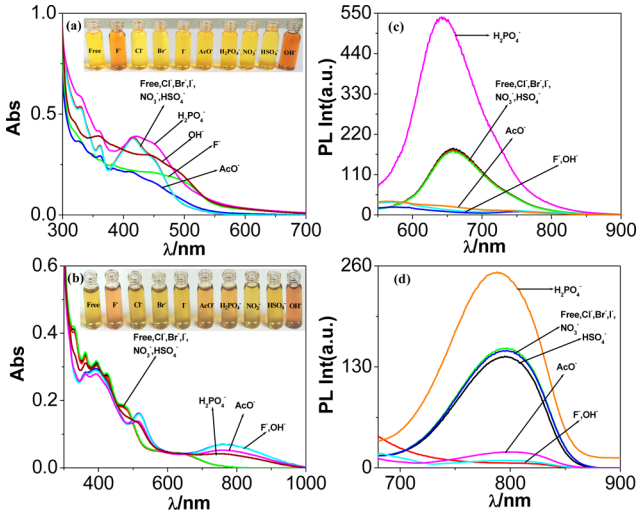

Figure 10. Changes in the UV−vis absorption and luminescence spectra of complex **1** (a and c, respectively) and complex **2** (b and d, respectively) in acetonitrile upon the addition of different anions as their TBA salts. The inset shows visible color changes that occur when the solutions of **1** (a) and **2** (b) are treated with various anions.

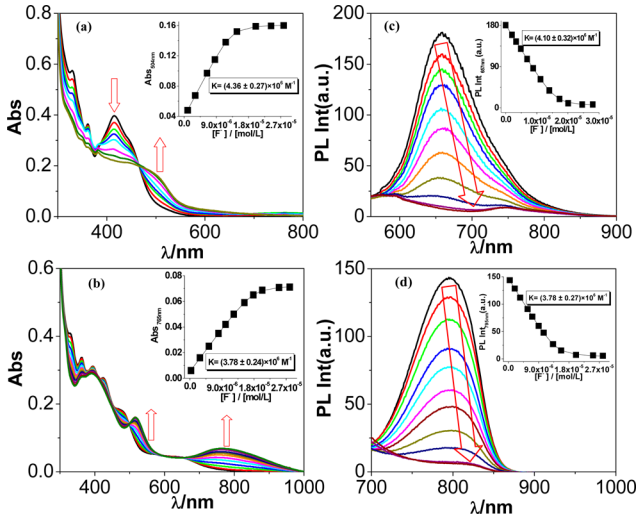

Figure 11. Changes in the UV−vis absorption and luminescence spectra of complexes **1** (a and c, respectively) and **2** (b and d, respectively) in an acetonitrile solution upon the addition of the F^- ion. The inset shows the fit of the experimental absorbance and luminescence data to a 1:1 binding profile.

The selective recognition of the anions by the metalloreceptors **1** and **2** was monitored through changes in their UV−vis absorption and emission spectral profiles. Parts a and b of Figure 10 indicate that the MLCT bands at 416 and 448 (sh) nm for **1** and at 476 nm and 654 (br) nm for **2** remain almost unaltered upon the addition of 1 equiv of Cl^-, Br^-, I^-, NO_3^-, and HSO_4^- ions. By contrast, similar to F^-, AcO^- and $H_2PO_4^-$ lead the MLCT bands to get red-shifted to the 452−504 nm region for **1** and to the 518 and 771 (br) nm regions for **2**. Parts c and d of Figure 10 shows that the luminescent band (658 nm for **1** and 796 nm for **2**) remains unchanged with all of the anions except F^-, AcO^-, and $H_2PO_4^-$. F^- and AcO^- ions completely quenched the emission of both receptors, while $H_2PO_4^-$ leads to the augmentation of the emission intensity in both cases.

Quantitative data for the interactions between the metalloreceptors and anions were obtained by systematic absorption and emission titration processes. Parts a and b of Figure 11 represent the absorption titration profiles of **1** and **2**, respectively, with respect to F^-. The MLCT peaks at 416 and 448 nm (sh) for **1** diminishes in intensity, and a new broad peak appeared at 504 nm, while for **2**, two new peaks at 518 and 771 nm are generated at the expense of the MLCT band at 476 nm. In both cases, 1 equiv of F^- was required for saturation, and all of the curves go through well-defined isosbestic point(s) (468 nm for **1** and 657, 587, and 500 nm for **2**). Figures S8 and S9 in the SI present the changes in the spectral patterns induced by the AcO^- ion. Spectral responses of receptor **1** toward $H_2PO_4^-$ indicate that the bands in the UV and visible regions are increased in intensity with the appearance of an isosbestic point at 420 nm, while for **2**, the MLCT band at 476 nm diminishes with the simultaneous appearance of two new bands at 517 nm (^{1}MLCT) and 771 nm (^{3}MLCT) accompanied by three isosbestic points at 654, 593, and 500 nm (Figure 12a,b). The calculated equilibrium constants for these interaction processes are roughly of 6 orders in magnitude (Table 4).

Photoluminescence titrations of **1** and **2** with F^- and AcO^- ions (Figures 11 and S10 and S11 in the SI) show almost

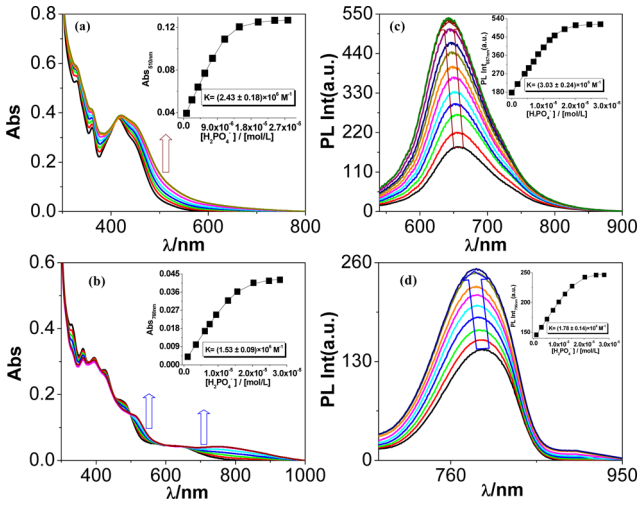

Figure 12. Changes in the UV−vis absorption and luminescence spectra of complexes **1** (a and c, respectively) and **2** (b and d, respectively) in an acetonitrile solution upon the addition of the $H_2PO_4^-$ ion. The inset shows the fit of the experimental absorbance and luminescence data to a 1:1 binding profile.

complete quenching of luminescence at 658 nm for **1** and 796 nm for **2** with concomitant red shift. By contrast, with the $H_2PO_4^-$ ion, a significant increase in the emission intensities occurs in both cases (Figure 12). The lifetimes of **1** in the presence of $H_2PO_4^-$ and F^- ions are represented in Figure 13. In the absence of anions, the decay profile of **1** is double-exponential in nature with lifetimes τ_1 = 6.8 ns and τ_2 = 78.0 ns. With increasing concentration of the F^- ion, the lifetimes of both components decrease, albeit to different extents, as shown in Figure 13. By contrast, with the $H_2PO_4^-$ ion, the lifetimes of both components increase substantially (from 6.8 to 76.0 ns for τ_1 and from 78.0 to 175.0 ns for τ_2). It may be mentioned that the steady-state and time-resolved luminescence behavior of **1** goes in the same direction. Thus, complex **1** can also act as a suitable lifetime-based sensor for F^- and $H_2PO_4^-$. The absorption and emission spectral behaviors of complexes with

DOI: 10.1021/ic502271k
Inorg. Chem. 2015, 54, 513−526

Table 4. Equilibrium Constants[a,b] ($K/10^6$ M^{-1}) for 1 and 2 toward Various Anions in an Acetonitrile Solution at 298 K

From Absorption Spectra		
	compound	
anion	1	2
F^-	4.36	3.78
AcO^-	2.13	3.40
$H_2PO_4^-$	2.43	1.68
OH^-	5.16	4.06
From Emission Spectra		
	compound	
anion	1	2
F^-	4.10	3.78
AcO^-	3.64	3.33
$H_2PO_4^-$	3.03	1.78
OH^-	4.42	3.86

[a] *tert*-Butyl salts of the respective anions were used for the studies. [b] Estimated errors were <15%.

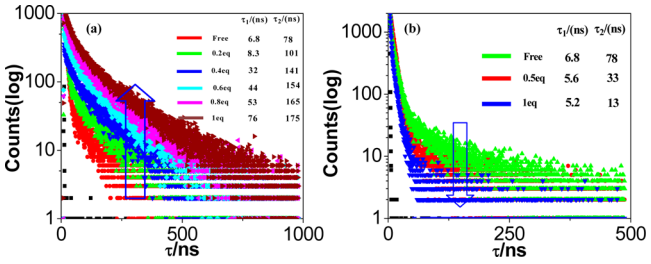

Figure 13. Changes in the time-resolved luminescence decays for **1** with the incremental addition of $H_2PO_4^-$ (a) and F^- (b) ions in an acetonitrile solution. The insets show the lifetime values.

OH^- (Figures S12 and S13 in the SI) are very similar to those of F^- and AcO^-, indicating NH proton abstraction by the said anions. Thus, quenching of the luminescence intensity occurs probably via an intramolecular photoinduced electron-transfer mechanism from the deprotonated ImzPPy to the excited-state metal centers caused by deprotonation of the NH proton of the imidazole moiety.[59] The augmentation of the emission intensity in the presence of $H_2PO_4^-$, on the other hand, is due to the rigidity imparted in the system through hydrogen-bonding interaction between the imidazole NH proton and $H_2PO_4^-$ ion.[59,83−86] Moreover, the different absorption and emission spectral responses of the complexes obtained for AcO^- and $H_2PO_4^-$ are due to their differences in basicity and size. From our previous works, it has been established that deprotonation phenomena predominate over hydrogen-bonding interactions when the anions are strongly basic in nature.[59] Such a possibility has already been explored here by observing the spectral changes of the metalloreceptors with TBAOH (Figures S12 and S13 in the SI). Thus, the AcO^- ion like F^- will tend to abstract the NH proton of the complexes, albeit to a lesser extent. On the other hand, besides hydrogen-bonding interaction between $H_2PO_4^-$ and imidazolyl NH of the metalloreceptors, the augmentation of emission in the presence of $H_2PO_4^-$ is possibly due to the excited-state protonation of **1** and **2** to some degree because $H_2PO_4^-$ is acidic in nature compared to the other anions such as AcO^-. Thus, the different interaction mechanisms of the metalloreceptors with the anions make them suitable "on−off" luminescence sensors for F^-, AcO^-, and OH^- ions with a quenching factor of ∼19 for **1** and a factor of ∼18 for **2** and potential "off−on" sensors for $H_2PO_4^-$ with an enhancement factor of ∼3 for **1** and a factor of ∼1.8 for **2** in the presence of 1 equiv of the said anions. The detection limits of **1** and **2** for F^-, AcO^-, and $H_2PO_4^-$ ions were calculated from spectrophotometric and fluorometric titration data, and the values are found to vary within the range of 3.73 × 10^{-9}−4.98 × 10^{-9} M (Table 5).[59]

DFT and TD-DFT Computations. Electronic structures of both the complexes and their deprotonated forms were characterized through computational studies in a solution phase. The optimized geometries for the complexes are presented in Figure S26 in the SI, and the geometrical parameters have already been given in Table 1. In general, there is a good correlation between the optimized structures and X-ray crystal structures of the complexes. Distortions from the perfect octahedral geometries of the complexes are also reflected in their calculated structures (Table 1).

The frontier molecular orbitals (MOs) of the complexes are represented in Figures S27 and S28 in the SI, while Table 6 summarizes their compositions and energies. Calculated results indicate that the pyrenylimidazole moiety is more electron-rich in the highest occupied molecular orbital (HOMO) for **1** and in both the HOMO and HOMO−1 for **2**, while HOMO−1, HOMO−2, and HOMO−3 for **1** and HOMO−2 and HOMO−3 for **2** show a large density on the metal and can thus be assigned to the metal t_{2g} orbitals, as is typically found for six-coordinated ruthenium(II) and osmium(II) polypyridine complexes.[87−91] The electron density in lowest unoccupied molecular orbital (LUMO) and LUMO+1, on the other hand, is mainly localized on the bpy moiety in both complexes. By contrast, in LUMO+2 and LUMO+3, the electron density mainly resides on the pyridine ring and pyrenylimidazole moiety connected to it in both complexes. Calculated results also indicate that NH deprotonation of the imidazole moiety leads to subtle changes in the frontier orbitals in both complexes.

The TD-DFT study was performed to predict the electronic absorption spectra of the complexes. The calculated spectral data along with the probable assignments of the bands are summarized in Table 7. The characters of the excited states have been designated as intraligand charge transfer (ILCT), MLCT, $\pi-\pi^*$, or ligand-to-ligand charge transfer (LLCT) depending on the involvement of the MOs in the transition processes. Energy level diagrams for the MOs involved in the transition processes of electrons are represented in Figures 14

Table 5. Spectrophotometric and Fluorimetric Detection Limits of 1 and 2 in an Acetonitrile Solution at 298 K

	detection limit/10^{-9} M					
	F^-		AcO^-		$H_2PO_4^-$	
compound	absorption	emission	absorption	emission	absorption	emission
1	4.29	4.98	4.68	4.89	3.75	3.93
2	4.55	4.34	4.51	4.68	3.73	3.60

DOI: 10.1021/ic502271k
Inorg. Chem. 2015, 54, 513−526

Table 6. Selected MO along with Their Energies and Compositions for 1, 1a, 2, and 2a in the Solution Phase

			% composition							
	energy/eV		1				1a			
MO	1	1a	Ru^{II}	pyrenylimidazole	py	bpy	Ru^{II}	pyrenylimidazole	py	bpy
LUMO+3	−1.83	−1.57	1.09	91.81	5.60	1.95	2.7	0.63	4.04	92.75
LUMO+2	−2.40	−1.63	4.69	33.96	49.36	12.35	3.59	31.47	61.78	3.17
LUMO+1	−2.51	−2.32	5.24	3.45	4.67	86.13	6.11	0.41	0.19	93.27
LUMO	−2.57	−2.39	2.69	1.70	3.18	92.56	3.90	0.18	0.46	95.47
HOMO	−5.72	−5.05	7.23	86.62	4.81	1.02	5.22	85.19	8.75	0.65
HOMO−1	−6.03	−5.58	74.52	12.39	3.09	10.24	56.33	35.53	0.12	7.469
HOMO−2	−6.17	−5.70	72.31	11.43	3.03	13.1	74.71	7.92	4.75	12.63
HOMO−3	−6.28	−5.92	78.25	1.23	3.22	17.27	76.21	3.03	3.34	17.31
			% composition							
	energy/eV		2				2a			
MO	2	2a	Os^{II}	pyrenylimidazole	py	bpy	Os^{II}	pyrenylimidazole	py	bpy
LUMO+3	−1.85	−1.58	1.15	84.66	7.78	6.41	3.62	4.40	6.30	85.26
LUMO+2	−2.40	−1.68	7.18	27.33	38.16	27.33	3.92	26.93	58.76	11.31
LUMO+1	−2.51	−2.30	8.06	5.25	6.47	80.2	9.09	0.55	0.32	89.99
LUMO	−2.62	−2.42	1.97	6.52	11.45	80.05	4.59	0.58	1.41	93.46
HOMO	−5.65	−5.05	47.51	40.46	4.44	7.58	15.63	73.45	7.74	2.47
HOMO−1	−5.84	−5.40	33.4	57.76	3.61	5.21	55.14	34.91	0.83	9.37
HOMO−2	−5.94	−5.48	69.93	9.20	4.29	16.57	68.31	10.00	5.97	15.76
HOMO−3	−6.06	−5.72	73.3	1.72	4.00	20.96	71.64	2.49	3.85	22.01

Table 7. Selected UV−Vis Energy Transitions at the TD-DFT/B3LYP Level for 1, 1a, 2, and 2a in Acetonitrile

excited state	λ_{cal}/nm (ε_{cal}/M^{-1} cm^{-1}), eV	oscillator strength (f)	λ_{expt}/nm (ε_{expt}/M^{-1} cm^{-1}), eV	key transitions	character
			Compound **1**		
S_3	465 (12620), 2.66	0.106	448 (br) (14995), 2.76	H−1 → L+2 (51%), H → L+2 (32%), H → L (6%)	MLCT, ILCT
S_9	420 (42610), 2.95	0.164	416 (br) (20310), 2.98	H−3 → L (38%), H−3 → L+1 (11%), H−3 → L+2 (11%), H−1 → L+2 (10%), H → L+2 (15%), H−2 → L+1 (8%)	MLCT
S_{15}	349 (17780), 3.55	0.080	362 (sh) (18290), 3.42	H → L+3 (34%), H → L+4 (11%), H−4 → L (3%), H−4 → L+2 (8%), H−1 → L+10 (9%)	ILCT, $\pi-\pi^*$
S_{27}	327 (31970), 3.79	0.079	332 (sh) (28935), 3.73	H−4 → L+2 (10%), H−1 → L+8 (20%), H → L+8 (28%), H−3 → L+4 (7%), H → L+3 (6%)	MLCT, LLCT, $\pi-\pi^*$
S_{53}	278 (131660), 4.46	0.159	286 (88038), 4.33	H−6 → L+2 (24%), H−4 → L+4 (30%), H−7 → L (9%), H−7 → L+1 (8%), H−7 → L+2, H−6 → L+1 (7%)	$\pi-\pi^*$
S_{97}	232 (108000), 5.34	0.358	239 (80225), 5.18	H−4 → L+9 (35%), H−1 → L+15 (17%), H−2 → L+11 (7%), H → L+15 (9%)	$\pi-\pi^*$
1a					
S_6	481 (10180), 2.57	0.031	496 (br) (8416), 2.49	H−3 → L+1 (14%), H−2 → L+1 (48%), H−1 → L+1 (20%), H−2 → L (8%)	MLCT, ILCT
S_{59}	278 (57940), 4.46	0.177	292 (54248), 4.24	H−8 → L (14%), H−1 → L+9 (26%), H−8 → L+1 (9%), H−7 → L+1 (6%), H−4 → L+4 (7%), H−4 → L+6 (7%)	$\pi-\pi^*$
S_{107}	234 (59840), 5.29	0.306	235 (55590), 5.27	H−4 → L+9 (28%), H → L+18 (25%), H−5 → L+9 (9%), H → L+16 (5%)	$\pi-\pi^*$
			Compound **2**		
S_8	444 (22710), 2.79	0.103	495 (br) (9577), 2.50	H−3 → L (20%), H−3 → L+1 (24%), H−2 → L+2 (34%), H−1 → L+1 (9%)	MLCT, ILCT
S_{27}	334 (30050), 3.71	0.042	362 (br) (14560), 3.42	H−2 → L+6 (56%), H−2 → L+7 (13%), H−3 → L+3 (9%)	MLCT
S_{55}	275 (82320), 4.51	0.495	290 (53400), 4.27	H−7 → L+1 (10%), H−6 → L+1 (12%), H−6 → L+2 (41%), H−7 → L (6%), H−7 → L+2 (8%)	$\pi-\pi^*$
S_{103}	231 (70020), 5.37	0.423	240 (71080), 5.16	H−9 → L+2 (11%), H−6 → L+5 (13%), H−4 → L+9 (39%), H−6 → L+7 (9%)	$\pi-\pi^*$
			Compund **2a**		
S_7	480 (19700), 2.58	0.166	520 (8410), 2.38	H−3 → L (69%), H−3 → L+1 (14%), H−2 → L+1 (7%)	MLCT
S_{20}	371 (31500), 3.34	0.152	395 (br) (14960), 3.13	H−4 → L (20%), H → L+4 (16%), H → L+7 (21%), H−3 → L+2 (8%), H → L+6 (9%)	LLCT, $\pi-\pi^*$
S_{61}	275 (86700), 4.51	0.471	290 (45720), 4.27	H−8 → L (13%), H−7 → L+1 (37%), H−4 → L+6 (19%), H−8 → L+1 (8%)	$\pi-\pi^*$
S_{107}	234 (84400), 5.29	0.196	235 (51500), 5.27	H−6 → L+6 (22%), H−6 → L+7 (18%), H−4 → L+9 (11%), H−5 → L+9 (5%), H−1 → L+15 (4%), H → L+15 (9%)	$\pi-\pi^*$

DOI: 10.1021/ic502271k
Inorg. Chem. 2015, 54, 513−526

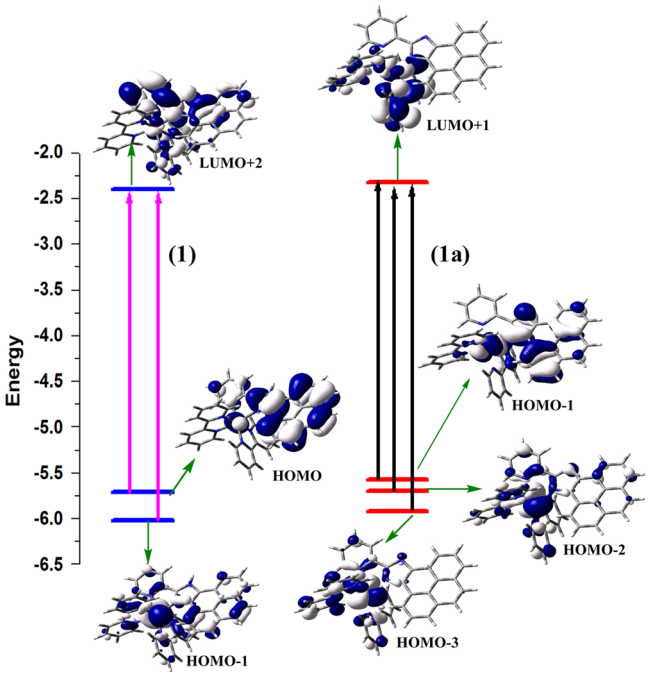

Figure 14. Energy level diagrams depicting the dominant transitions that comprise the lowest-energy absorption band for $[(bpy)_2Ru(HImzPPy)]^{2+}$ (**1**) and $[(bpy)_2Ru(ImzPPy)]^{+}$ (**1a**) in acetonitrile.

and 15. Overlays of the calculated and experimental spectra of the complexes are portrayed in Figure 16. The calculated

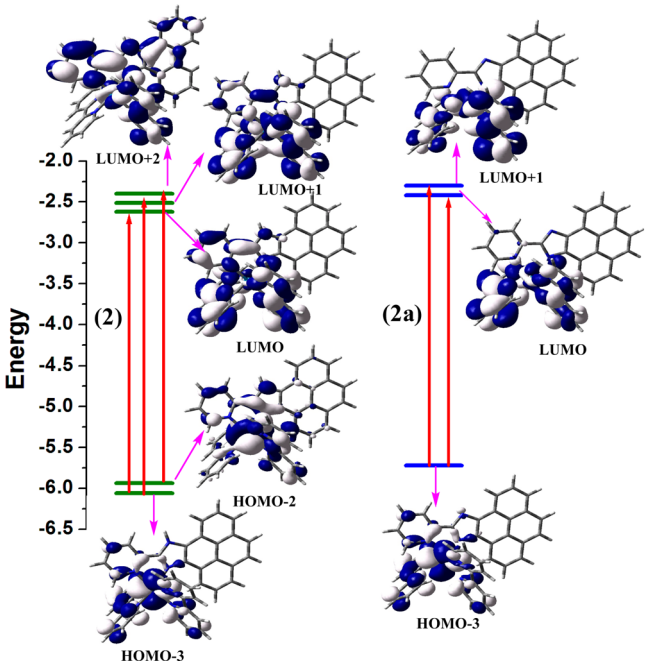

Figure 15. Energy level diagrams depicting the dominant transitions that comprise the lowest-energy absorption band for $[(bpy)_2Os(HImzPPy)]^{2+}$ (**2**) and $[(bpy)_2Os(ImzPPy)]^{+}$ (**2a**) in acetonitrile.

spectra display the expected MLCT band in the visible region, as well as the $\pi-\pi^*$ transitions in the UV region for both complexes. For example, the simulated spectra indicate a peak at 465 nm for **1** and at 444 nm for **2** with oscillator strengths (f) 0.106 and 0.103, respectively, in the visible region. These

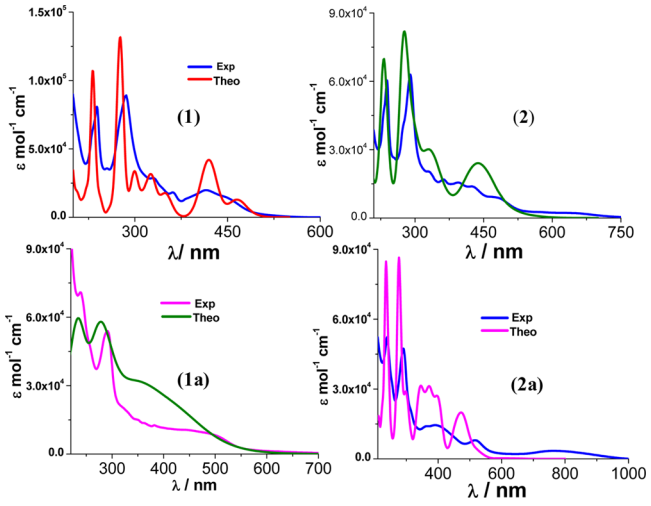

Figure 16. Calculated and experimental absorption spectra of **1**, **1a**, **2**, and **2a** in acetonitrile at RT.

spin-allowed transitions predominantly originated from the metal-based HOMO to the bpy-based LUMO charge-transfer (MLCT) processes, although some ILCT character arising from the pyrenylimidazole moiety to the Py group of HImzPPy is also involved therein. The calculated bands at 420 nm with f = 0.164 for **1** and at 334 nm with f = 0.042 for **2** are also due to the MLCT process. Furthermore, strong bands in the UV region most likely originated from the transitions within the π orbitals of bpy and HImzPPy and are predominantly $\pi-\pi^*$ in character. Computed and experimental data obtained for the absorption spectra of both protonated and deprotonated forms of the complexes match qualitatively well in terms of both the peak positions and relative optical density in acetonitrile (Table 7). Theoretically, we get a shift of about 1−51 nm compared to that of the experimental bands, which is quite good with respect to TD-DFT calculations for the transition-metal complexes.[87−91] Again, the shift of the MLCT bands toward higher wavelengths upon deprotonation is also well reproduced from our calculations.

The optimized geometries of the complexes in the T_1 state using the TD-DFT method are presented in Figure S29 in the SI along with the related geometrical data in Table S5 in the SI. The selected frontier MOs of the complexes in the triplet excited state are represented in Figures S30 and S31 in the SI. Optimized geometries of the complexes differ to a very small extent in both the ground (S_0) and excited (T_1) states. The vertical gap between T_1 and S_0 gives the calculated emission energies of the complexes (Table S6 in the SI). The plots of the frontier MOs responsible for the emission processes are displayed in Figures S32 and S33 in the SI. Calculated emission bands at 705 nm for **1** and 758 nm for **2**, originating from the lowest-energy T_1 state, correspond well to their experimental values at 658 nm for **1** and 796 nm for **2**, respectively (Table S6 in the SI). On the basis of the compositions of HOMOs and LUMOs in the triplet states, the calculated emissions can be assigned as the transitions from the ^{3}MLCT state. Finally, the red shift observed in the experimental λ_{emi} of the complexes due to NH deprotonation are in line with our computations.

CONCLUSIONS

In summary, we reported a new class of monometallic ruthenium(II) and osmium(II) complexes based on π-

DOI: 10.1021/ic502271k
Inorg. Chem. 2015, 54, 513−526

expansive pyrenylpyridylimidazole ligands as efficient DNA intercalators and anion sensors. X-ray crystallographic study provides the unambiguous structures of the complexes in the solid state, whereas the structures in the solution state were determined by NMR and ESI-MS. Although we expected the ruthenium(II) dyad derived from a π-expansive pyrene chromophore should exhibit a long lifetime corresponding to its ^{3}LC and/or ^{3}ILCT state, detailed luminescence measurements suggest that the traditional luminescence from the ^{3}MLCT state are predominantly operative in both cases and are only slightly affected by the extended conjugation of the pyrene moiety. The results of different spectroscopic measurements indicate conclusively that the mode of binding of the metal complexes with CT-DNA is intercalative in nature with the binding constant on the order of 10^6 M^{-1}. The increased affinity of the complexes toward DNA was ascribed to a planar and extended conjugation of the pyrenylimidazole ligand present in the complexes. Moreover, significant enhancement of the luminescence quantum yields and lifetimes of the aqueous solution of the complexes in the presence of CT-DNA justify their molecular "light-switch" behaviors. Interestingly, the present complexes have been found to be useful in sensing selective anions such as F^-, AcO^-, and $H_2PO_4^-$ in solution owing to the presence of the imidazole NH proton in their second coordination sphere. The anion-sensing studies showed that the complexes act as "turn-on" luminescence sensors for $H_2PO_4^-$ owing to probable hydrogen-bonding interaction and "turn-off" sensors for F^- and AcO^- ions owing to the deprotonation of the imidazole NH proton present in the complexes. Additionally, DFT and TD-DFT calculations on the complexes and their deprotonated forms were also carried out to gain better insight into their electronic structures and excited-state properties. Good correlations between the experimental and theoretical results help us to assign the main absorption and emission behaviors of the complexes.

■ ASSOCIATED CONTENT

Supporting Information

X-ray crystallographic data in CIF format, ^{1}H−^{1}H COSY NMR, ESI-MS, UV−vis absorption, steady-state and time-resolved luminescence spectra, and MO picture spectra related to DFT and TD-DFT calculations (Figures S1−S33 and Tables S1−S6). This material is available free of charge via the Internet at http://pubs.acs.org.

■ AUTHOR INFORMATION

Corresponding Author

*E-mail: sbaitalik@hotmail.com.

Notes

The authors declare no competing financial interest.

■ ACKNOWLEDGMENTS

The authors thank CSIR (India) as well as DST (India) for financial support through Grants 01(2766)/13/EMR-II and SR/S1/IC 33/2010 for this work. THe single-crystal XRD facility under DST-FIST and the TCSPC facility under the DST-PURSE program of Department of Chemistry (JU) are gratefully acknowledged. S.M. thanks the UGC, while S.K. and D.M. acknowledge the CSIR for their research fellowship.

■ REFERENCES

(1) (a) Balzani, V.; Credi, A.; Venturi, M. *Molecular Devices and Machines*; Wiley-VCH: Weinheim, Germany, 2003. (b) Baitalik, S.; Wang, X.; Schmehl, R. H. *J. Am. Chem. Soc.* **2004**, *126*, 16304−16305. (c) Browne, W. R.; O'Boyle, N. M.; McGarvey, J. J.; Vos, J. G. *Chem. Soc. Rev.* **2005**, *34*, 641−649. (d) Manner, V. W.; DiPasquale, A. G.; Mayer, J. M. *J. Am. Chem. Soc.* **2008**, *130*, 7210−7211. (e) Manner, V. W.; Mayer, J. M. *J. Am. Chem. Soc.* **2009**, *131*, 9874−9875.

(2) (a) Juris, A.; Balzani, V.; Barigelletti, F.; Campagna, S.; Belser, P.; von Zelewsky, A. *Coord. Chem. Rev.* **1988**, *84*, 85−277. (b) Balzani, V.; Juris, A.; Venturi, M.; Campagna, S.; Serroni, S. *Chem. Rev.* **1996**, *96*, 759−834. (c) Medlycott, E. A.; Hanan, G. S. *Chem. Soc. Rev.* **2005**, *34*, 133−146.

(3) Meyer, T. J. *Acc. Chem. Res.* **1989**, *22*, 163−170.

(4) Kelly, O.; Barton, J. K. In *Metal Ions in Biological Systems*; Sige, A., Sigel, H., Eds.; Marcel Dekker: New York, 1999; Vol. 39, p 211.

(5) Erkkila, K. E.; Odom, D. T.; Barton, J. K. *Chem. Rev.* **1999**, *99*, 2777−2795.

(6) Kirsch-De Mesmaeker, A.; Lecomte, J.-P.; Kelly, J.-M. *Top. Curr. Chem.* **1996**, *177*, 25.

(7) Pyle, A. M.; Barton, J. K. In *Progress in Inorganic Chemistry*; Lippard, S. J., Ed.; Wiley-Interscience: New York, 1990; Vol. *38*, pp 413−474.

(8) Sigman, D. S.; Mazumder, A.; Perrin, D. M. *Chem. Rev.* **1993**, *93*, 2295−2316.

(9) Friedman, A. E.; Chambron, J.-C.; Sauvage, J.-P.; Turro, N. J.; Barton, J. K. *J. Am. Chem. Soc.* **1990**, *112*, 4960−4962.

(10) Dupureur, C. M.; Barton, J. K. *J. Am. Chem. Soc.* **1994**, *116*, 10286−10287.

(11) Dupureur, C. M.; Barton, J. K. *Inorg. Chem.* **1997**, *36*, 33−43.

(12) Jenkins, Y.; Friedman, A. E.; Turro, N. J.; Barton, J. K. *Biochemistry* **1992**, *31*, 10809−10 816.

(13) (a) Holmlin, R. E.; Barton, J. K. *Inorg. Chem.* **1995**, *34*, 7−8. (b) Holmlin, R. E.; Yao, J. A.; Barton, J. K. *Inorg. Chem.* **1999**, *38*, 174−189. (c) Holmlin, R. E.; Stemp, E. D. A.; Barton, J. K. *J. Am. Chem. Soc.* **1996**, *118*, 5236−5244.

(14) Hudson, B. P.; Dupureur, C. M.; Barton, J. K. *J. Am. Chem. Soc.* **1995**, *11*, 9379−9380.

(15) Barton, J. K. *Science* **1986**, *233*, 727−734.

(16) Lincoln, P.; Broo, A.; Norden, B. *J. Am. Chem. Soc.* **1996**, *118*, 2644−2653.

(17) Tuite, E.; Lincoln, P.; Norden, B. *J. Am. Chem. Soc.* **1997**, *119*, 239−240.

(18) Norden, B.; Lincoln, P.; Akerman, B.; Tuite, E. In *Metal Ions in Biological Systems*; Sigel, A., Sigel, H., Eds.; Marcel Dekker: New York, 1996; Vol. *33*, pp 177−252.

(19) (a) Westerlund, F.; Pierard, F.; Eng, M. P.; Norden, B.; Lincoln, P. *J. Phys. Chem. B* **2005**, *109*, 17327−17332. (b) Lundin, N. J.; Walsh, P. J.; Howell, S. L.; McGarvey, J. J.; Blackman, A. G.; Gordon, K. C. *Inorg. Chem.* **2005**, *44*, 3551−3560. (c) Boer, D. R.; Wu, L.; Lincoln, P.; Coll, M. *Angew. Chem.* **2014**, *53*, 1949−1952. (d) Andersson, J.; Fornander, L. H.; Abrahamsson, M.; Tuite, E.; Nordell, P.; Lincoln, P. *Inorg. Chem.* **2013**, *52*, 1151−1159.

(20) (a) Chouai, A.; Wicke, S. E.; Turro, C.; Bacsa, J.; Dunbar, K. R.; Wang, D.; Thummel, R. P. *Inorg. Chem.* **2005**, *44*, 5996−6003. (b) Liu, Y.; Hammitt, R.; Lutterman, D. A.; Thummel, R. P.; Turro, C. *Inorg. Chem.* **2007**, *46*, 6011−6021. (c) Sun, Y.; Lutterman, D. A.; Turro, C. *Inorg. Chem.* **2008**, *47*, 6427−6434. (d) Sun, Y.; Joyce, L. E.; Dickson, N. M.; Turro, C. *Chem. Commun.* **2010**, *46*, 6759−6761. (e) Monro, S.; Scott, J.; Chouai, A.; Lincoln, R.; Zong, R.; Thummel, R. P.; McFarland, S. A. *Inorg. Chem.* **2010**, *49*, 2889−2900.

(21) Kane-Maguire, N. A. P.; Wheeler, J. F. *Coord. Chem. Rev.* **2001**, *211*, 145−162.

(22) Kaes, C.; Katz, A.; Hosseini, M. W. *Chem. Rev.* **2000**, *100*, 3553−3590.

(23) (a) Bhat, S. S.; Kumbhar, A. S.; Lönnecke, P.; Hawkins, E. H. *Inorg. Chem.* **2010**, *49*, 4843−4853. (b) Bhat, S. S.; Kumbhar, A. S.; Kumbhar, A. A.; Khan, A. *Chem.—Eur. J.* **2012**, *18*, 16383−16392.

(24) Ambroise, A.; Maiya, B. G. *Inorg. Chem.* **2000**, *39*, 4256−4263.

DOI: 10.1021/ic502271k
Inorg. Chem. 2015, 54, 513−526

(25) Ambroise, A.; Maiya, B. G. *Inorg. Chem.* **2000**, *39*, 4264−4272.
(26) Mariappan, M.; Maiya, B. G. *Eur. J. Inorg. Chem.* **2005**, 2164−2173.
(27) (a) Howarth, A. J.; Majewski, M. B.; Wolf, M. O. *Coord. Chem. Rev.* DOI: 10.1016/j.ccr.2014.03.024. (b) Stephenson, M.; Reichardt, C.; Pinto, M.; Wachtler, M.; Sainuddin, T.; Shi, G.; Yin, H.; Monro, S.; Sampson, E.; Dietzek, B.; McFarland, S. A. *J. Phys. Chem. A* DOI: 10.1021/jp504330s.
(28) Mardanya, S.; Karmakar, S.; Das, S.; Baitalik, S. *Sens. Actuators, B* **2015**, *206*, 701−713.
(29) Han, M.-J.; Gao, L.-H.; Wang, K.-Z. *New J. Chem.* **2006**, *30*, 208−214.
(30) Xu, H.; Zheng, K.-C.; Chen, Y.; Li, Y.-Z.; Lin, L.-J.; Li, H.; Zhang, P.-X.; Ji, L.-N. *J. Chem. Soc., Dalton Trans.* **2003**, 2260−2268.
(31) Tan, L.-F.; Chao, H.; Li, H.; Liu, Y.-J.; Sun, B.; Wei, W.; Ji, L.-N. *J. Inorg. Biochem.* **2005**, *99*, 513−520.
(32) Xiong, Y.; Ji, L.-N. *Coord. Chem. Rev.* **1999**, *185*−*186*, 711−733.
(33) Ji, L.-N.; Zou, X.-H.; Liu, J.-G. *Coord. Chem. Rev.* **2001**, *216*−*217*, 513−536.
(34) Zhen, Q.-Z.; Ye, B.-H.; Zhang, Q.-L.; Liu, J.-G.; Li, H.; Ji, L.-N.; Wang, L. *J. Inorg. Biochem.* **1999**, *76*, 47−53.
(35) Wu, J.-Z.; Ye, B.-H.; Wang, L.; Ji, L.-N.; Zhou, J.-Y.; Li, R.-H.; Zhou, Z.-Y. *J. Chem. Soc., Dalton Trans.* **1997**, 1395−1401.
(36) Liu, F. R.; Wang, K. Z.; Bai, G. Y.; Zhang, Y. A.; Gao, L. H. *Inorg. Chem.* **2004**, *43*, 1799−1806.
(37) Han, M. J.; Gao, L. H.; Lü, Y. Y.; Wang, K. Z. *J. Phys. Chem. B* **2006**, *110*, 2364−2371.
(38) Chen, Y. M.; Liu, Y. J.; Li, Q.; Wang, K. Z. *J. Inorg. Biochem.* **2009**, *103*, 1359.
(39) Ma, Y. Z.; Yin, H. J.; Wang, K. Z. *J. Phys. Chem. B* **2009**, *113*, 11039−11047.
(40) Zhang, A.-G.; Zhang, Y.-Z.; Duan, Z.-M.; Wang, K.-Z.; Wei, H.-B.; Bian, Z.-Q.; Huang, C.-H. *Inorg. Chem.* **2011**, *50*, 6425−6436.
(41) Zhao, X.-L.; Li, Z.-S.; Zheng, Z.-B.; Zhang, A.-G.; Wang, K.-Z. *Dalton Trans.* **2013**, *42*, 5764−5777.
(42) (a) Wrighton, M. S.; Morse, D. L.; Pdungsap, L. *J. Am. Chem. Soc.* **1975**, *97*, 2073−2079. (b) Ford, W. E.; Rodgers, M. A. J. *J. Phys. Chem.* **1992**, *96*, 2917−2920. (c) Wilson, G. J.; Launikonis, A.; Sasse, W. H. F.; Mau, A. W.-H. *J. Phys. Chem. A* **1998**, *102*, 5150−5156.
(43) (a) Grusenmeyer, T. A.; Chen, J.; Jin, Y.; Nguyen, J.; Rack, J. J.; Schmehl, R. H. *J. Am. Chem. Soc.* **2012**, *134*, 7497−7506. (b) Simon, J. A.; Curry, S. L.; Schmehl, R. H.; Schatz, T. R.; Piotrowiak, P.; Jin, X.; Thummel, R. P. *J. Am. Chem. Soc.* **1997**, *119*, 11012−11022.
(44) Tyson, D. S.; Castellano, F. N. *J. Phys. Chem. A* **1999**, *103*, 10955−10960.
(45) McClenaghan, N. D.; Leydet, Y.; Maubert, B.; Indelli, M. T.; Campagna, S. *Coord. Chem. Rev.* **2005**, *249*, 1336−1350.
(46) Sohna Sohna, J. E.; Carrier, V.; Fages, F.; Amouyal, E. *Inorg. Chem.* **2001**, *40*, 6061−6063.
(47) Ji, S.; Wu, W.; Wu, W.; Guo, H.; Zhao, J. *Angew. Chem., Int. Ed.* **2011**, *50*, 1626−1629.
(48) (a) Morales, A. F.; Accorsi, G.; Armaroli, N.; Barigelletti, F.; Pope, S. J. A.; Ward, M. D. *Inorg. Chem.* **2002**, *41*, 6711−6719. (b) Maubert, B.; McClenaghan, N. D.; Indelli, M. T.; Campagna, S. *J. Phys. Chem. A* **2003**, *107*, 447−455. (c) McClenaghan, N. D.; Barigelletti, F.; Maubert, B.; Campagna, S. *Chem. Commun.* **2002**, *6*, 602−603.
(49) Sessler, J. L.; Gale, P. A.; Cho, W. S. *Anion Receptor Chemistry*; Royal Society of Chemistry: Cambridge, U.K., 2006.
(50) Martínez-Máñez, R.; Sancenón, F. *Chem. Rev.* **2003**, *103*, 4419−4476.
(51) (a) Peŕez, J.; Riera, L. *Chem. Commun.* **2008**, 533−543. (b) Peŕez, J.; Riera, L. *Chem. Soc. Rev.* **2008**, *37*, 2658−2667.
(52) Steed, J. W. *Chem. Soc. Rev.* **2009**, *38*, 506−519.
(53) (a) Beer, P. D. *Chem. Commun.* **1996**, 689−696. (b) Beer, P. D.; Gale, P. A. *Angew. Chem., Int. Ed.* **2001**, *40*, 486−516. (c) Sessler, J. L.; Davis, J. M. *Acc. Chem. Res.* **2001**, *34*, 989−997.
(54) Amendola, V.; Fabbrizzi, L. *Chem. Commun.* **2009**, 513−531.
(55) dos Santos, C. M. G.; Harte, A. J.; Quinn, S. T.; Gunnlaugsson, T. *Coord. Chem. Rev.* **2008**, *252*, 2512−2527.
(56) Rice, C. R. *Coord. Chem. Rev.* **2006**, *250*, 3190−3199.
(57) (a) Bowman-James, K. *Acc. Chem. Res.* **2005**, *38*, 671−678. (b) Sun, S.-S.; Lees, A. J. *Coord. Chem. Rev.* **2002**, *230*, 171−192. (c) Bondy, C. R.; Loeb, S. J. *Coord. Chem. Rev.* **2003**, *240*, 77−99. (d) de Silva, A. P.; Gunaratne, H. Q. N.; Gunnlaugsson, T.; Huxley, A. J. M.; McCoy, C. P.; Rademacher, J. T.; Rice, T. E. *Chem. Rev.* **1997**, *97*, 1515−1566.
(58) (a) Yam, V. W. W.; Ko, C. C.; Zhu, N. *J. Am. Chem. Soc.* **2004**, *126*, 12734−12735. (b) Yam, V. W. W. *Acc. Chem. Res.* **2002**, *35*, 555−563.
(59) (a) Bhaumik, C.; Das, S.; Saha, D.; Dutta, S.; Baitalik, S. *Inorg. Chem.* **2010**, *49*, 5049−5062. (b) Bhaumik, C.; Saha, D.; Das, S.; Baitalik, S. *Inorg. Chem.* **2011**, *50*, 12586−12600. (c) Bhaumik, C.; Das, S.; Maity, D.; Baitalik, S. *Dalton Trans.* **2012**, *41*, 2427−2438. (d) Saha, D.; Das, S.; Maity, D.; Dutta, S.; Baitalik, S. *Inorg. Chem.* **2011**, *50*, 46−61. (e) Saha, D.; Das, S.; Bhaumik, C.; Dutta, S.; Baitalik, S. *Inorg. Chem.* **2010**, *49*, 2334−2348. (f) Maity, D.; Bhaumik, C.; Mondal, D.; Baitalik, S. *Inorg. Chem.* **2013**, *52*, 13941−13955. (g) Maity, D.; Bhaumik, C.; Mardanya, S.; Karmakar, S.; Baitalik, S. *Chem.—Eur. J.* **2014**, *20*, 13242−13252. (h) Das, S.; Karmakar, S.; Mardanya, S.; Baitalik, S. *Dalton Trans.* **2014**, *43*, 3767−3782.
(60) Hu, J.; Zhang, D.; Harris, F. W. *J. Org. Chem.* **2005**, *70*, 707−708.
(61) Sullivan, B. P.; Meyer, T. J. *Inorg. Chem.* **1978**, *17*, 3334−3341.
(62) Lay, P. A.; Sargeson, A. M.; Taube, H. *Inorg. Synth.* **1986**, *24*, 291.
(63) Lanter, J. C. *Encycl. Reagents Org. Synth.* **2001**, DOI: 10.1002/047084289X.rs026.
(64) Perrin, D. D.; Armarego,W. L. F. *Purification of Laboratory Chemicals*, 3rd ed.; Pergamon: New York, 1988.
(65) ORTEP-32 for Windows: Farrugia, L. J. *J. Appl. Crystallogr.* **1997**, *30*, 565−566.
(66) Rillema, D. P.; Blanton, C. B.; Shaver, R. J.; Jackman, D. C.; Boldaji, M.; Bundy, S.; Worl, L. A.; Meyer, T. J. *Inorg. Chem.* **1992**, *31*, 1600−1606.
(67) Nair, R. B.; Teng, E. S.; Kirkand, S. L.; Murphy, C. J. *Inorg. Chem.* **1998**, *37*, 139−141.
(68) (a) Cater, M. T.; Rodriguez, M.; Bard, A. J. *J. Am. Chem. Soc.* **1989**, *111*, 8901−8911. (b) Smith, S. R.; Neyhart, G. A.; Karlsbeck, W. A.; Thorp, H. H. *New J. Chem.* **1994**, *18*, 397−406.
(69) (a) Friedman, A. E.; Kumar, C. V.; Turro, N. J.; Barton, J. K. *Nucleic Acids Res.* **1991**, *19*, 2595−2602. (b) Kumar, C. V.; Barton, J. K.; Turro, N. J. *J. Am. Chem. Soc.* **1985**, *107*, 5518−5523. (c) Pyle, A. M.; Rehmann, J. P.; Meshoyrer, R.; Kumar, C. V.; Turro, N. J.; Barton, J. K. *J. Am. Chem. Soc.* **1991**, *111*, 3051−3058.
(70) (a) Hiort, C.; Lincoln, P.; Norden, B. *J. Am. Chem. Soc.* **1993**, *115*, 3448−3454. (b) Phillips, T.; Haq, I.; Meijer, A. J. H. M.; Adams, H.; Soutar, I.; Swanson, L.; Sykes, M. J.; Thomas, J. A. *Biochemistry* **2004**, *43*, 13657−13665.
(71) (a) Boisdenghien, A.; Moucheron, C.; Kirsch-De Mesmaeker, A. *Inorg. Chem.* **2005**, *44*, 7678−7685. (b) Leveque, J.; Elias, B.; Moucheron, C.; Kirsch-De Mesmaeker, A. *Inorg. Chem.* **2005**, *44*, 393−400. (c) Moucheron, C.; Kirsch-De Mesmaeker, A.; Choua, S. *Inorg. Chem.* **1997**, *36*, 584−592.
(72) (a) Tysoe, S. A.; Kopelman, R.; Schelzig, D. *Inorg. Chem.* **1999**, *38*, 5196−5197. (b) Liu, Y.; Chouai, A.; Degtyareva, N. N.; Lutterman, D. A.; Dunber, K. R.; Turro, C. *J. Am. Chem. Soc.* **2005**, *127*, 10796−10797.
(73) Hartshorn, R. M.; Barton, J. K. *J. Am. Chem. Soc.* **1992**, *114*, 5919−5925.
(74) (a) Brennaman, M. K.; Alstrum-Acevedo, J. H.; Fleming, C. N.; Jang, P.; Meyer, T. J.; Papanikolas, J. M. *J. Am. Chem. Soc.* **2002**, *124*, 15094−15098. (b) Bernnaman, M. K.; Meyer, T. J.; Panpanikolas, J. M. *J. Phys. Chem. A* **2004**, *108*, 9938−9944. (c) Gholamkhass, B.; Koike, K.; Negishi, N.; Hori, H.; Takeuchi, K. *Inorg. Chem.* **2001**, *40*, 756−765. (d) Liu, J. G.; Zhang, Q. L.; Shi, X. F.; Ji, L. N. *Inorg. Chem.* **2001**, *40*, 5045−5050.

DOI: 10.1021/ic502271k
Inorg. Chem. 2015, 54, 513−526

(75) Nair, R. B.; Murphy, C. J. *J. Inorg. Biochem.* **1998**, *69*, 129−133.
(76) Ortmans, I.; Elias, B.; Kelly, J. M.; Moucheron, C.; Kirsch-DeMesmaeker, A. *Dalton Trans.* **2004**, 668−676.
(77) (a) Patel, D. J. *Acc. Chem. Res.* **1979**, *12*, 118−125. (b) Patel, D. J.; Canuel, L. L. *Proc. Natl. Acad. Sci. U.S.A.* **1976**, *73*, 3343−3347. (c) Berman, H. M.; Young, P. A. *Annu. Rev. Biophys. Bioeng.* **1981**, *10*, 87−114.
(78) Boger, D. L.; Fink, B. E.; Brunette, S. R.; Tse, W. C.; Hedrick, M. P. *J. Am. Chem. Soc.* **2001**, *123*, 5878−5891.
(79) Baguley, B. C.; Falkenhaug, E. M. *Nucleic Acids Res.* **1978**, *5*, 161−171.
(80) (a) Lyng, R.; Härd, T.; Norden, B. *Biopolymers* **1987**, *26*, 1327−1345. (b) Norden, B.; Tjerneld, F. *Biopolymers* **1982**, *21*, 1713−1734. (c) Schipper, P. E.; Norden, B.; Tjerneld, F. *Chem. Phys. Lett.* **1980**, *70*, 17−21.
(81) (a) Duff, M. R.; Tan, W. B.; Bhambhani, A.; Perrin, B. S., Jr.; Thota, J.; Rodger, A.; Kumar, C. V. *J. Phys. Chem. B* **2006**, *110*, 20693−20701. (b) Modukuru, N. K.; Snow, K. J.; Perrin, B. S., Jr.; Thota, J.; Kumar, C. V. *J. Phys. Chem. B* **2005**, *109*, 11810−11818. (c) Rodger, A.; Taylor, S.; Adlam, G.; Blagbrough, I. S.; Haworth, I. S. *Bioorg. Med. Chem.* **1995**, *3*, 861−872.
(82) Haq, I.; Jenkins, T. C.; Chowdhry, B. Z.; Ren, J. S.; Chaires, J. B. *Methods Enzymol.* **2000**, *323*, 373−405.
(83) Zheng, Z.-B.; Duan, Z.-M.; Ma, Y.-Y.; Wang, K.-Z. *Inorg. Chem.* **2013**, *52*, 2306−2316.
(84) (a) Lazarides, T.; Miller, T. A.; Jeffery, J. C.; Ronson, T. K.; Adams, H.; Ward, M. D. *Dalton Trans.* **2005**, 528−536. (b) Mo, H. J.; Niu, Y. L.; Zhang, M.; Qiao, Z.-P.; Ye, B. H. *Dalton Trans.* **2011**, *40*, 8218−8225. (c) Mo, H.-J.; Wu, J.-J.; Qiao, Z.-P.; Ye, B.-H. *Dalton Trans.* **2012**, *41*, 7026−7036.
(85) (a) Kitchen, J. A.; Boyle, E. M.; Gunnlaugsson, T. *Inorg. Chim. Acta* **2012**, *381*, 236−242. (b) Beer, P. D.; Graydon, A. R.; Sutton, L. R. *Polyhedron* **1996**, *15*, 2457−2461. (c) Duff, T.; Grussing, A.; Thomas, J.-L.; Duati, M.; Vos, J. G. *Polyhedron* **2003**, *22*, 775−780.
(86) Hargrove, E.; Nieto, S.; Zhang, T.; Sessler, J. L.; Anslyn, E. V. *Chem. Rev.* **2011**, *111*, 6603−6782.
(87) Vlcek, A.; Zalis, S. *Coord. Chem. Rev.* **2007**, *251*, 258−287.
(88) Daul, C.; Baerends, E. J.; Vernooijs, P. *Inorg. Chem.* **1994**, *33*, 3538−3543.
(89) Nazeeruddin, M. K.; De Angelis, F.; Fantacci, S.; Selloni, A.; Viscardi, G.; Liska, P.; Ito, S.; Bessho, T.; Grätzel, M. *J. Am. Chem. Soc.* **2005**, *127*, 16835−16847.
(90) (a) Wächtler, M.; Kupfer, S.; Guthmuller, J.; Pop, J.; González, L.; Dietzek, B. *J. Phys. Chem. C* **2011**, *115*, 24004−24012. (b) Kupfer, S.; Guthmuller, J.; Wächtler, M.; Losse, S.; Rau, S.; Dietzek, B.; Popp, J.; Gonzalez, L. *Phys. Chem. Chem. Phys.* **2011**, *13*, 15580−15588. (c) Atsumi, M.; Gonzalez, L.; Daniel, C. *J. Photochem. Photobiol., A* **2007**, *190*, 310−320.
(91) (a) Monat, J. E.; Rodriguez, J. H.; McCusker, J. K. *J. Phys. Chem. A* **2002**, *106*, 7399−7406. (b) Wang, J.; Bai, F.-Q.; Xia, B.-H.; Sun, L.; Zhang, H.-X. *J. Phys. Chem. A* **2011**, *115*, 1985−1991. (c) Rekhis, M.; Labat, F.; Ouamerali, O.; Ciofini, I.; Adamo, C. *J. Phys. Chem. A* **2007**, *111*, 13106−13111. (d) Fantacci, S.; De Angelis, F.; Selloni, A. *J. Am. Chem. Soc.* **2003**, *125*, 4381−4387.

DOI: 10.1021/ic502271k
Inorg. Chem. 2015, 54, 513−526